FNP

JOURNAL OF FOOD PROCESS ENGINEERING

D.R. HELDMAN
EDITOR

FOOD & NUTRITION PRESS, INC.

VOLUME 8, NUMBER 1 QUARTERLY

JOURNAL OF FOOD PROCESS ENGINEERING

All articles for publication and inquiries regarding publication should be sent to Prof. D. R. Heldman, Campbell Institute for Research and Technology, Campbell Place, Camden, New Jersey 01810 USA.

All subscriptions and inquiries regarding subscription should be sent to Food & Nutrition Press, Inc., 155 Post Road East, P.O. Box 71, Westport, Connecticut 06881 USA.

One volume of four issues will be published annually. The price for Volume 8 is $70.00 which includes postage to U.S., Canada, and Mexico. Subscriptions to other countries are $82.00 per year via surface mail, and $90.00 per year via airmail.

Subscriptions for individuals for their own personal use are $50.00 for Volume 8 which includes postage to U.S., Canada, and Mexico. Personal subscriptions to other countries are $62.00 per year via surface mail, and $70.00 per year via airmail. Subscriptions for individuals should be sent to the publisher and marked for personal use.

The *Journal of Food Process Engineering* (ISSN 0145-8876) is published quarterly (March, June, September and December) by Food & Nutrition Press, Inc.—Office of Publication is 155 Post Road East, P.O. Box 71, Westport, Connecticut 06881 USA. (Current issue is September 1985).

Second class postage paid at Westport, CT 06881.

POSTMASTER: Send address changes to Food & Nutrition Press, Inc., 155 Post Road East, P.O. Box 71, Westport, CT 06881.

JOURNAL OF FOOD PROCESS ENGINEERING

JOURNAL OF FOOD PROCESS ENGINEERING

Journal of
FOOD PROCESS ENGINEERING

VOLUME 8
NUMBER 1

Editor: D. R. HELDMAN

FOOD & NUTRITION PRESS, INC.
WESTPORT, CONNECTICUT 06881 USA

Food & Nutrition Press, Inc.
Westport, Connecticut USA

ISSN 0145-8876

Printed in the United States of America

CONTENTS

MEETINGS

September, 1985

9/9–9/12 International Symposium on Processing and Aseptic Packaging. Sponsored by IUFOST Food Working Party of the European Federation of Chemical Engineering. Tylosand, Sweden. Contact Kurssekretariatet, Lund Institute of Technology, P.O. Box 118, S-22100, Lund, Sweden.

9/15–9/20 Fourth International Conference on Packaging. Michigan State University. East Lansing, Michigan. Contact R. C. Griffin, Jr., School of Packaging, Michigan State University, East Lansing, Michigan 48824.

November, 1985

11/8–11/12 International Baking Industry Exposition. Las Vegas, Nevada. Contact Ibea c/o Aba, 2020 K Street, NW Suite 850, Washington, D.C. 20006.

11/10–11/14 Winter Annual Meeting of the American Institute of Chemical Engineers. Palmer House, Chicago, Illinois. Contact Beth Van Dijk, AIChE, 345 E. 47th Street, New York, N. Y. 10017.

December, 1985

12/11–12/13 First IFAC Symposium on Modelling and Control of Biotechnological Processes. Noordwijkerhout, The Netherlands. Contact A. Mooser, Royal Institute of Engineers in the Netherlands, P.O. Box 30424, 2500 GK, The Haige, The Netherlands.

12/17–12/20 Winter Meeting of the American Society of Agricultural Engineers. Hyatt Regency-Chicago, Illinois. Contact M. A. Purschwitz, American Society of Agricultural Engineers, 2950 Niles Road—P. O. Box 410, St. Joseph, Michigan 49085.

MODELING A TWIN SCREW CO-ROTATING EXTRUDER[1]

W. A. YACU[2]
RHM Research Limited
Lincoln Road
High Wycombe, Bucks. HP12 3QR.
England

Submitted for publication: March 30, 1984
Accepted for publication: October 10, 1984

ABSTRACT

This work desribes the simulation of a twin screw co-rotating extruder. Based on a uni-directional analysis, the temperature and pressure profiles within the extruder are predicted from knowledge of feed and extruder characteristics. A non-Newtonian, non-isothermal viscosity model is used to describe the materials rheology. The analysis covers an evaluation of conditions within the solid conveying zone, the melt pumping zone and a melt shearing zone achieved by reverse screw elements. The total energy input (both mechanical and through the barrel) is also evaluated. The simulation work has proved satisfactory in the design and optimization of extruder operation.

INTRODUCTION

Very little work has been published about the mechanisms of material flow and energy transfer in intermeshing co-rotating extruders. Most of this work (Burkhardt *et al.* 1978; Denson and Hwang 1980; Wyman 1975) treated the melt flow in a similar way to that of a single screw extruder as a combination of drag and pressure flows. Booy (1980) added a third flow element due to the pushing action of the second screw in the intermeshing region. All these assumed a Newtonian and isothermal fluid. Another approach (Olkko *et al.* 1980) has been the analysis of process response variables by multiple regression methods. While this approach achieves information about the specific process and product properties, it does not provide engineering understanding of the interactions between the extruder

[1]Based on a paper presented on the COST 91 Concluding Seminar, Athens, Greece, November 14-18, 1983.

[2]Current Address: Baker Perkins (BCS) Limited, Westfield Rd., Peterborough, PE3 6TA, England.

Journal of Food Engineering 8 (1985) 1-21.

design, the material's characteristics and the operating conditions of the extruder. Greater understanding of the flow mechanism seems to exist in intermeshing counter-rotating extruders. This has been based on the axial movement of material in closed C-shaped chambers (Burkhardt *et al.* 1978; Janssen 1978).

The present work is primarily concerned with the evaluation of the temperature and pressure profiles in the axial direction (parallel to the screw shaft). This then serves as the basic information required for the evaluation of the extruder performance.

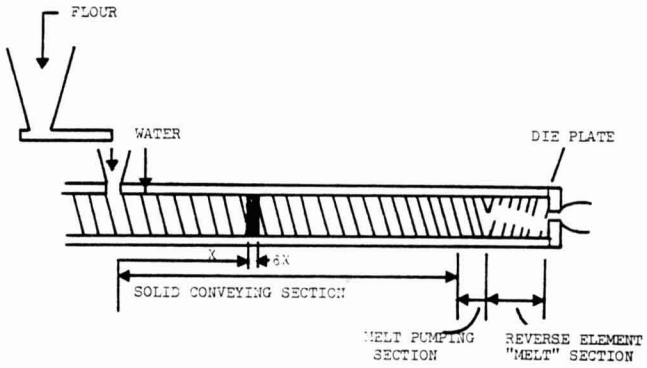

FIG. 1. SCHEMATIC DIAGRAM OF THE EXTRUDER

A schematic diagram of the extruder is presented in Fig. 1. The extruder analysis covers the solid conveying zone, the melt pumping zone and a melt shearing zone caused by reverse screw elements fitted at the end of the shaft before the die plate. The following assumptions are made: (1) The food melt rheology is described by a non-Newtonian, non-isothermal viscosity model taking into consideration the effect of moisture and fat content. (2) Steady state behavior and uniform conditions in the direction normal to the screw shaft. (3) The melt flow is highly viscous and in the laminar flow regime. (4) Gravity effects are negligible and are ignored. (5) Heat losses to the screw shafts are neglected. (6) Only the net flow in the axial direction is considered.

Twin screw extruders mostly operate under starved feed conditions and the throughput is determined by the feeding unit and the extruder's screw speed and torque limit. The actual length of the melt pumping section will accordingly constitute only part of the screw length. It will be affected by the screw design, the screw speed, throughput, material's viscosity and the overall flow resistance. The material's temperature increases rapidly along the melt section causing a change in its viscosity. This prevents the straightforward calculaton of the required pressure and hence the length of the melt pumping section. A trial and error approach is therefore adopted. This is

based on starting with the best estimate of the melt pumping section length, evaluating the temperature profile first and then the pressure profile.

The pressure drop across the die plate hole is evaluated independently using the product temperature achieved at that stage and the specific die characteristics. If this die pressure is higher or lower than that evaluated earlier at the die plate, the pumping section length is increased or decreased respectively and the evaluation procedure started again. This calculation continues until the acceptable accuracy tolerance is obtained.

THEORETICAL TREATMENT

Temperature Profile

The Solid Conveying Section. As explained earlier, twin screw extruders are normally starve-fed and therefore the screws in this section are only partially full and no pressure is developed. Therefore, negligible viscous heat dissipation takes place. If required, heat can be transferred to the powder through the barrel, this is expected to take place by conduction. To simplify the analysis, convection heat transfer is assumed. A pseudo-heat transfer coefficient U_s is used to replace the characteristic conductivity property (k/l). This approach is realistic owing to the fact that mixing within the channel is reasonably good in co-rotating extruders. Constructing a heat balance across an element normal to the axial direction and solving for T with the boundary condition at $\chi = 0$ $T = T_f^o$ results (Eq. 1 and 2):

$$QC_{vs}T + \upsilon U_s A(T_{bi} - T)\delta\chi = QC_{vs}(T + dT) \tag{1}$$

$$T = T_{bi} - (T_{bi} - T_f^o)\, e^{-\frac{\upsilon U_s A}{QC_{vs}}\chi} \tag{2}$$

The value of U_s was found to be much lower than that predicted by the penetration theory (Harriott 1959). This is because of phase discontinuity and the existence of additional resistance to heat transfer between the solid particles. υ describes the degree of screw filling which increases with decreasing the screw pitch (Janssen 1978).

The Melt Pumping Section. The change of material from solid powder to fluid melt is assumed to take place in a sudden change. From the experimental observations, this assumption was found to be realistic. The screws become completely full in this section. In order to construct and evaluate a heat balance across an element in this zone, it is necessary first to describe the way the mechanical energy is consumed. Part of this energy is converted to thermal heat (including melting and heat of reaction, if any) and potential

energy within the product. The kinetic energy is relatively small and can be ignored. Martelli (1982) estimated the energy converted to thermal heat by viscous dissipation per screw channel in one screw turn. He assumed that heat was dissipated within the channel and due to leakage flow in the various gaps. These were (1) between the flight tip of the screw and the inside surface of the barrel, (2) between the flight tip of one screw and the bottom of the channel of the other and (3) between the flights of opposite screws parallel to each other.

The heat dissipation within the channel was estimated by (Eq. 3):

$$Z_1 = \mu\gamma^2 V_p \tag{3}$$

where V_p is the channel volume and was estimated as (Eq. 4):

$$V_p = \frac{\pi^2}{2} D \cdot D_e \, h \tan\theta_p \tag{4}$$

D_e is the equivalent twin screw diameter estimated as (Eq. 5):

$$D_e = \frac{2}{\pi}(\pi D - \sqrt{2Dh}) \tag{5}$$

The shear rate within the channel only was estimated as (Eq. 6):

$$\gamma = \frac{\pi D_e N}{h} \tag{6}$$

Substituting Eq. 4-6 in Eq. 3 results (Eq. 7):

$$Z_1 = \frac{\pi^4 D_e^3 D \tan\theta_p}{2h} \mu N^2 \tag{7}$$

Based on a force balance, the power dissipation within a clearance space was derived (McKelevey 1962; Schenkel 1966), as (Eq. 8):

$$dZ = \frac{\mu u^2}{c} dA \tag{8}$$

Martelli (1982) defined the relative product velocity (u) within the various clearances and calculated their resultant energy dissipation per one channel in one screw turn. For a screw with an (m) number of flight starts these can be described as follows:

(1) between the flight tip of the screw and the inside surface of the barrel (Eq. 9):

$$Z_2 = \frac{\pi^2 D^2 e C_e}{\alpha} m\mu N^2 \tag{9}$$

C_e is the equivalent twin screw circumference and was estimated by (Eq. 10):

$$C_e = 2(\pi D - \sqrt{2Dh}) \tag{10}$$

(2) between the flight tip of one screw and the bottom of the channel of the other (Eq. 11):

$$Z_3 = \frac{8\pi^2 I^3 e}{\epsilon} m\mu N^2 \tag{11}$$

(3) between the flights of opposite screws parallel to each other (Eq. 12):

$$Z_4 = \frac{\pi^2 I^2 h \sqrt{D^2 - I^2}}{2\sigma} m\mu N^2 \tag{12}$$

The total energy per channel per one screw turn was therefore expressed as (Eq. 13 and 14):

$$Z_p = Z_1 + Z_2 + Z_3 + Z_4 \tag{13}$$

$$= C_{1p}\mu_p N^2 \tag{14}$$

where C_{1p} can be termed as the pumping section screw geometry factor and is described as (Eq. 15):

$$C_{1p} = \frac{\pi^4 D_e^3 D \tan\theta p}{2h} + m\left(\frac{\pi^2 D^2 e C_e}{\alpha} + \frac{8\pi^2 I^3 e}{\epsilon} + \frac{\pi^2 I^2 h \sqrt{D^2 - I^2}}{2\sigma}\right) \tag{15}$$

The amount of heat generated within an element of $\delta\chi$ thickness can be therefore evaluated as (Eq. 16):

$$dZ_p = C_{1p}\mu_p N^2 \frac{\delta\chi}{\pi D \tan\theta_p} \tag{16}$$

The overall shear rate the product is exposed to while passing through the pumping zone (including that due to leakage flows) can be estimated by assimilating Eq. 14 with Eq. 3 (Eq. 17 and 18):

$$\mu_p \gamma_p^2 V_p = C_{1p} \mu_p N^2 \tag{17}$$

$$\therefore \gamma_p = N \sqrt{\frac{C_{1p}}{V_p}} \tag{18}$$

The product apparent viscosity μ_p will be described by power low and a dependence on temperature, moisture content and fat content as follows (Eq. 19 and 20):

$$\mu_p = \mu_o e^{-a_1(MC-MC^o)} e^{-a_2 F} \gamma_p^{-n_1} e^{-bT} \tag{19}$$

$$= \mu_1 \gamma_p^{-n_1} e^{-bT} \tag{20}$$

Further discussion of the viscosity and shear rate definition is given in the Rheology Characteristics section of this work. μ_1 is the initial viscosity after accounting for moisture and fat content. At a given screw speed, this can be further reduced to (Eq. 21 and 22):

$$\mu_p = \mu_{2p} e^{-bT} \tag{21}$$

where

$$\mu_{2p} = \mu_1 \gamma_p^{-n_1} \tag{22}$$

Constructing a heat balance across an element in the melt pumping zone (Eq. 23 through 26):

$$QC_{vm}T + U_m A(T_{bi} - T)d\chi + \frac{C_{1p}\mu_{2p}N^2 e^{-bT}}{\pi D \tan\theta_p} d\chi = QC_{vm}(T + dT) \tag{23}$$

or

$$\frac{dT}{d\chi} = C_{2p} e^{-bT} + C_{3p}(T_{bi} - T) \tag{24}$$

where

$$C_{2p} = \frac{C_{1p}\mu_{2p}N^2}{\pi D \tan\theta_p Q C_{vm}} \tag{25}$$

and

$$C_{3p} = \frac{U_m A}{QC_{vm}} \tag{26}$$

Equation 24 is a first order, nonlinear differential equation. Coupled with the boundary condition: $T = T^o_m$ at $\chi = \chi^o_m$, it can be integrated numercially by the Simpson 3/8 rule (Jenson and Jeffreys 1977).

The Reverse Element Section. The mechanism of fluid flow and heat generation within this section are extremely complicated and no relevant work could be cited. The existence of cross channels normal to the screw

channel (in some cases) adds further to this complication. These cross channels are introduced in order to improve mixing and reduce the total sheer stress. The net flow in this section is necessarily equal to that of the melt pumping zone. As a reasonable approximation, the heat generation by viscous dissipation is assumed to take place much in the same way as in the melt pumping section. The presence of cross channels is accounted for by modifying the screw geometry factor C_{1r} (equivalent to C_{1p} defined by Eq. 15) in the following way (Eq. 27):

$$C'_{1r} = C_{1r}\left(1 - \frac{m_1 BG}{\pi Dh}\right) \tag{27}$$

The screws remain full in this section. A heat balance across this section can therefore be described as follows (Eq. 28):

$$QC_{vm}T + U_m A(T_{bi} - T)d\chi + \frac{C'_{1r}\mu_r N^2}{\pi D \tan\theta_r} d\chi - QdP = QC_{vm}(T + dT) \tag{28}$$

$-QdP$ is the energy dissipated due to pressure drop. The pressure gradient in this section is estimated from a formula having a similar structure to that of the fluid pressure gradient in the annulus between two concentric pipes (Bird *et al.* 1960). (Eq. 29):

$$\frac{dP}{d\chi} = -\frac{Q\mu_r}{K_1} \tag{29}$$

where K_1 is the screw conductance and is approximated by (Eq. 30):

$$K_1 = \frac{h^5 \tan\theta_r}{D(1 - m_1 BG/\pi Dh)} \tag{30}$$

The apparent viscosity in this section (μ_r) is described in a similar way to that of the melt pumping section (Eq. 31):

$$\mu_r = \mu_1 \gamma_r^{-n} e^{-bT} \tag{31}$$

Substituting Eq. 29 and 31 in Eq. 28 and rearranging, (Eq. 32):

$$\frac{dT}{d\chi} = (C_{2r} + C_{4r})e^{-bT} + C_{3r}(T_{bi} - T) \tag{32}$$

where C_{2r} and C_{3r} are similar to C_{2p} and C_{3p} described by Eq. 25 and 26 for the melt pumping section, and (Eq. 33):

$$C_{4r} = \frac{QD\mu_1\dot{\gamma}_r^{-n}(1 - m_1BG/\pi Dh)}{C_{vm}h^5\tan\theta_r} \tag{33}$$

Coupled with the boundary condition: $T = T_p^o$ at $\chi = X°_p$, Eq 32 is also solved numerically by the Simpson 3/8 rule integration method.

Pressure Profile

The screws are partially empty in the solid conveying zone. Therefore no pressure is developed at this stage.

The Melt Pumping Section. Considerable disagreement exists in the published literature over the definition of flow mechanism and the boundary conditions (Booy 1980; Burkhardt *et al.* 1978; Denson and Hwang 1980; Wyman 1975). Burkhardt *et al.* (1978), Denson and Hwang (1980) and Wyman (1975) calculated the volumetric flow rate by integrating the velocity vector v_z (in the channel direction) with respect to channel width and height in a similar way to that of a single screw extruder. Wyman (1975) however concluded that the flow due to pressure gradient had the same direction as that of the drag flow. In other words, the pressure gradient is negative in the z direction. This concept is hard to accept owing to the open nature of co-rotating screws and the existence of a continuous channel. Booy (1980) added a positive displacement flow element in the axial direction to account for the pushing action of the second screw in the intermeshing region. Generally it can be stated that the theory of fluid flow and the development of the pressure profile in co-rotating extruders is still in its early development stages. This is more so when accounting for specific extruder geometry and the fact that extruded materials are generally non-Newtonian undergoing considerable temperature changes.

A subjective and quantitative analysis of the pressure profile is followed in this work. This is based on theoretical input verified by experimental results. The length of the pumping section and the pressure generated behind the die plate were measured experimentally. The formula adopted and tested is that of the maximum pressure gradient (when the discharge end is closed) derived by Wyman (1975) (Eq. 34):

$$\left(\frac{dP}{dz}\right)_{max} = \frac{6\pi DN\mu_p \cos\theta_p}{h^2} \tag{34}$$

Assuming that a continuous channel exists, the pressure profile in the axial direction $dP/d\chi$ can be calculated as (Eq. 35):

$$\left(\frac{dP}{d\chi}\right) = \frac{dP}{dz} \cdot \frac{1}{\sin\theta_p} \cdot \frac{D_e}{D} \tag{35}$$

for a small h/D ratio Eq. 34, therefore reduces to (Eq. 36):

$$\left(\frac{dP}{d\chi}\right)_{max} = \frac{12\pi DN\mu_p}{h^2 \tan\theta_p} \tag{36}$$

Experimentally Eq. 36 was found to provide good prediction of the length and final pressure behind the die plate in our extruder when the constant value was replaced by 4. This is then solved for a non-Newtonian non-isothermal fluid whose apparent viscosity is defined by Eq. 21. Substituting and rearranging (Eq. 37 and 38):

$$\frac{dP}{d\chi} = K_2 e^{-bT} \tag{37}$$

where

$$K_2 = \frac{4\pi DN\mu_{2p}}{h^2 \tan\theta_p} \tag{38}$$

To simplify the solution of Eq. 37, T is defined as a function of χ (Eq. 39):

$$T = T^\circ_m + g_p(\chi - \chi_m) \tag{39}$$

Substituting Equation 39 in Equation 37 and solving for P with the boundary condition: $P = 0$ at $\chi = \chi^\circ_m$, the final pressure at $\chi = \chi^\circ_p$ is then calculated as (Eq. 40):

$$P_p = \frac{K_2 e^{-bT^\circ_m}}{bg_p} \left(1 - e^{-bg_p(\chi^\circ_p - \chi^\circ_m)}\right) \tag{40}$$

The Reverse Element Section

The pressure gradient in this section was defined by Eq. 29 as:

$$\frac{dP}{d\chi} = \frac{-Q\mu_r}{K_1} \tag{29}$$

substituting for μ_r by Eq. 31 and rewriting (Eq. 41):

$$\frac{dP}{d\chi} = \frac{-Q\mu_1\gamma_r^{-n}e^{-bT}}{K_1} \tag{41}$$

Similarly, defining T as a function of χ (Eq. 42):

$$T = T^\circ_p + g_r(\chi - \chi^\circ_p) \tag{42}$$

Substituting Eq. 42 in Eq. 41 and solving for P with the boundary condition: $P = P_p$ at $\chi = \chi_p$, (Eq. 43 and 44):

$$P = P^\circ_p - \frac{K_3}{bg_r}(1 - e^{-bg_r(\chi - \chi^\circ_p)}) \tag{43}$$

where

$$K_3 = \frac{Q\mu_1\gamma_r^{-n}e^{-bT_p}}{K_1} \tag{44}$$

Substituting L for χ in Eq. 43 the melt pressure at the end of this section can be evaluated.

Pressure Drop Across the Die Hole. This is calculated by (Eq. 45):

$$\Delta P = \frac{-Q\mu_d}{K_d} \tag{45}$$

From a force balance across the die plate, K_d for a circular hole can be defined as (Eq. 46):

$$K_d = \frac{\pi d^4}{128l} \tag{46}$$

Pressure drop due to entrance (end) effect is accounted for from experimental evaluation of the materials rheology (Harper 1981).

Rheology Characteristics

Rheology Model. The rheology model for a wheat A-starch was determined using the twin screw extruder itself as a capillary viscometer. Pressure drop measurements were carried out across three capillaries of

l/d ratio: 3, 4 and 6. The calculation procedure for capillary shear rate, end effect, the effect of moisture and fat is given in references (Cervone and Harper 1978; Chen *et al.* 1978; Harper 1981; Ramsen and Clark 1978). The value of the various indices was determined by Multiple Regression Analysis to fit the following rheology equation. The shear rate element (γ^{-n}) definition is dealt with in the next section. The general model for the apparent viscosity is described by Eq. 47:

$$\mu = \mu_o e^{-a_1(MC - MC^o)} e^{-a_2 F} \gamma^{-n} e^{-bT} \tag{47}$$

Definition of Shear Rate. The food material faces different kinds of shear regimes while passing through the melting zones of the extruder. It also undergoes considerable physical and chemical reactions which change its rheology irreversibly. Until more information is available about these reactions, empirical approximation seems the most practical way of describing the food rheology. From our work on the capillary rheology measurements using the extruder as a viscometer, it was found necessary to take into consideration the shear characteristics of the screws as well as those of the capillary. The rate of the physical/chemical reactions appeared to be affected by the shear rate within the extruder. The definition of the shear rate in the various melt sections of the extruder is therefore important as it could indirectly explain some of the material phase changes.

The Melt Pumping Section. The overall shear rate in this section γ_p was defined by Eq. 18. This was based on the summation of absolute values of the average shear rate within the channel and the various gaps. The effect of shear rate only on the apparent viscosity μ_p is predicted using the Ostwalde power law model (Eq. 48 and 49):

$$\mu = \mu^\circ \gamma_p^{-n_1} \tag{48}$$

or

$$\mu_p = \mu^\circ \left(N \sqrt{\frac{C_{1p}}{V_p}}\right)^{-n_1} \tag{49}$$

The Reverse Element Section. In this section, the average shear rate was first described in a similar way to that of fluid flow in the annulus between two concentric pipes. However, due to the non-Newtonian nature of food melts, it was decided to account also for the average shear rate caused by the screw rotation, i.e., Eq. 50:

$$\mu_r = \mu^\circ \gamma_p^{-n_2} \gamma_r^{-n_3} \tag{50}$$

where γ_p was defined by Eq. 18 and γ_r is estimated as (Eq. 51):

where
$$\gamma_r = \frac{QD(1 - m_1 BG/\pi Dh)}{h^4 \tan\theta_r} \tag{51}$$

Within The Die Hole. As mentioned earlier, it was found necessary to account for the average shear rate caused by the screw rotation as well as the axial average shear rate caused by the fluid flow within the capillary (Eq. 52).

$$\mu_d = \mu^\circ \gamma_p^{-n_2} \gamma_d^{-n_3} \tag{52}$$

where (Eq. 53):

$$\gamma_d = \frac{32Q}{\pi d^3} \tag{53}$$

The values of n_1, n_2, n_3 were estimated from a series of experiments evaluating the material's rheology. Different screw geometry and configuration (with and without the reverse element) were used. The rheology were correlated using multiple regression analysis.

Energy Requirement

Mechanical Energy Supplied by the Motor. This is calculated from knowledge of total viscous heat dissipation and potential energy developed within the extruder (Eq. 54):

$$\int_{\chi^\circ_m}^{L} dE = \int_{\chi^\circ_m}^{\chi^\circ_p} \frac{C_{1p} N^2 \mu_p d\chi}{\pi D \tan\theta_p} + \int_{\chi^\circ_p}^{L} \frac{C'_{1r} N^2 \mu_r d\chi}{\pi D \tan\theta_r} + \int_{P_a}^{P_d} Q dP \tag{54}$$

μ_p and μ_r were defined by Eq. 20 and 31, respectively. The temperature is then defined as a function of χ in a similar way to that carried out for evaluating the pressure profile in the Pressure Profile section. Solving Eq. 54 for E with the boundary conditions: $T = T_m$ at $\chi = \chi^\circ_m$ and $T = T^\circ_p$ at $\chi = \chi^\circ_p$ resulted in (Eq. 55, 56 and 57):

$$E = K_4(1 - e^{-bg_p(\chi^\circ_p - \chi^\circ_m)}) + K_5(1 - e^{-bg_r(L - \chi^\circ_p)}) + Q \cdot P_d \ldots \tag{55}$$

where $$K_4 = \frac{C_{1p}N^2\mu_{2p}e^{-bT^\circ_m}}{bg_p\pi D\tan\theta_p} \tag{56}$$

and $$K_5 = \frac{C'_{1r}N^2\mu_{2r}e^{-bT^\circ_p}}{bg_r\pi D\tan\theta_r} \tag{57}$$

Accounting for a motor efficiency factor ϵ, the total motor energy consumption E_T is (Eq. 58):

$$E_T = \frac{E}{\epsilon} \tag{58}$$

Energy Supplied or Taken by the Barrel. In most cases, heat is supplied or taken by the barrel according to a controlled temperature set point. In some cases, multiple zone temperature control is provided. The calculation will be confined here, as an example to the melt pumping zone. The total heat flow through the barrel is the summation of heat flow across all the individual heating/cooling zones.

Assuming that the controlled temperature is the inside barrel surface temperature T_{bi} and is constant along the melt pumping zone, the logarithmic mean temperature difference is (Eq. 59):

$$\Delta T_{lm} = \frac{T^\circ_p - T^\circ_m}{ln\left(\frac{T^\circ_{bi} - T^\circ_m}{T^\circ_{bi} - T^\circ_p}\right)} \tag{59}$$

Heat transfer to the material H_{1p} (Eq. 60):

$$H_{1p} = \pi D_e L_p U_m \Delta T_{lm} \tag{60}$$

This heat is equal to that transferred across the thickness of the barrel (assuming that both the heating and/or the cooling source are placed at the outside barrel surface). The outside barrel temperature (T_{bo}) is calculated assuming a symmetrical cylinder barrel of an inside diameter D_e and outside diameter D_O as (Eq. 61):

$$T_{bo} = T_{bi} + \frac{H_{1p}ln(D_o/D_e)}{2\pi kL_p} \tag{61}$$

Heat losses to the air, in the case of no insulation and no resistance to heat transfer between the heating bands and the barrel surface is estimated as (Eq. 62):

$$H_{2p} = \pi D_o L_p U_a (T_{bo} - T_a) \tag{62}$$

Total heat supplied through this section of the barrel H_t is then (Eq. 63):

$$H_{tp} = H_{1p} + H_{2p} \tag{63}$$

Total energy supply per unit throughput (Eq. 64):

$$(S) = \frac{E_T + H_T}{M} \tag{64}$$

EXPERIMENTAL INVESTIGATIONS

The twin screw extruder used in this work was fabricated by Almex B.V., Holland, to our specifications. It can be operated in the counter and co-rotating modes and its length be adjusted to give L/D ratio from 9/1 to 24/1. For this work, the L/D ratio was 12 and was operating in the co-rotating mode. The geometry details of the barrel and screw elements are given in Table 1.

The feed material (wheat A-starch) was fed by a vibrating screw feeder. Water was fed directly to the barrel and its flowrate was adjusted by a flow rotameter. Measured variables (at steady state for about 20 min) included: product pressure and temperature behind the die plate, barrel temperatures, screw speed and armature current of the motor. Owing to instrument limitations, the material temperature and pressure could not be measured along the barrel. In some selected experiments, the powder feeder, the water supply and the extruder were stopped simultaneously, the extruder cooled and the screw shafts pulled out for inspection.

RESULTS AND DISCUSSION

A computer program in the BASIC language was written to carry out the trial and error calculation and predict the extruder performance.

Using the physical properties and the rheology model data listed in Table 2, the predicted results were generally in reasonable agreement with

Table 1. Extruder geometry specifications.

Co-rotating twin screw extruder

Barrel: Length = 0.66m; Inside Diam. = 55mm; Outside Diam. = 130mm

Screw Channel Depth = 7mm

Screw Shafts Centre-Centre Distance = 48mm

Screw Configuration

	Screw Pitch,mm	No. of Starts	Length,cm
Feed Section 1	55	2	16.5
Feed Section 2	40	2	33.0
Pump Section	30	2	8.5
Reverse Section	30	2	8.0

Screw Details in the Pumping and Reverse Sections

e	1.8 mm
α	0.7 mm
ε	0.7 mm
δ	3.0 mm

Reverse screw cross channel: Width (B) 10 mm

Depth (G) 7 mm

No. of Channels (m_1) 3

Die Hole: Circular of 4mm diameter and 12mm long

Table 2. Physical properties, operating conditions and rheology data used in the modelling example.

A. Physical Properties and Operating Conditions

Material:

Wheat A-Starch, supplied by Tenstar Aquitaine, Bordeaux, France

	Solid Conveying Section	Melt Sections
Specific heat, kj/kg°C	1.7	2.7
Density, kg/m^3	700	1,400
Heat transfer coefficient, W/m^2°C	30	500
Feed temperature, °C	25	
Air temperature, °C	30	30
Natural convection heat Transfer coefficient, W/m^2°C	10	20
Barrel inside surface temp., °C	80	170
Screw speed, rps	2.5	
Feed rate, kg/hr	30.0	
Moisture content, %	16.0	
Fat content (ground nut oil), %	1.0	

B. Rheology Model Data

Initial viscosity μ_o, N.S./m^2	120,000
Reference moisture content MC°,%	6
Moisture coefficient a_1	0.07
Fat coefficient a_2	0.1
Temperature coefficient b	0.005
Shear rate (power law) index	
n_1	0.7
n_2	0.4
n_3	0.3

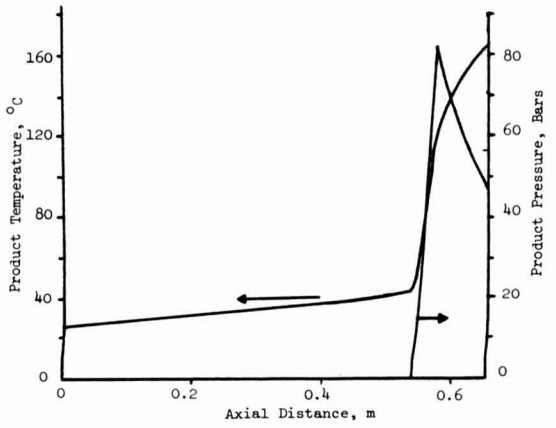

FIG. 2. PREDICTED TEMPERATURE AND PRESSURE PROFILES WITHIN THE EXTRUDER

Table 3. Predicted extruder performance results.

	Solid Conveying Section	Melt Pumping Section	Melt Reverse Section
Length, cm	54	4	8
Material final:			
Temp., °C	42	119	162
Pressure, 10^5 N/m^2	0	82	45
Viscosity, N.s/m^2		815	439 (392 within the die hole)
Barrel outside temp., °C	80.5	192	192
Energy supplied to the material, W-hr/kg			
i - By the motor (net)			
Thermal		39.5	21
Potential		1.6	-0.8
Motor efficiency at 65%			
Total (gross) energy supplied by the motor = 94 W-hr/kg			
ii - By the heating bands, W-hr/kg			
to the material	7.2	25.0	
lost to the air	3.7	1.8	
	10.9	26.8	
Total heater band energy supply = 38 W-hr/kg			
Total energy = 132 W-hr/kg			

Table 4. Comparison between measured and predicted results.

					Measured			Predicted		
Feed Rate kg/hr	Moisture Content %	Screw Speed rpm	Barrel Temp. °C	Die Hole Diameter mm	Pre-die Pressure 10^5N/m^2	Pre-die Material Temp.°C	Motor Current Amps	Pre-die Pressure 10^5N/m^2	Pre-die Material Temp.°C	Motor Current Amps
25.1	16.0	140	148	4	52.4	162	25	43.6	169	25
32.5	16.0	200	181	4	37.2	183	30	37.0	183	25
40.0	18.0	140	160	4	83.8	167	38	72.0	158	35
36.4	16.0	170	174	4	54.5	176	22	51.3	174	29
32.5	20.0	140	162	4	55.2	163	32	48.3	161	25
40.0	20.0	200	179	4	45.9	175	20	45.0	171	26
29.5	16.5	180	190	6	24.1	151	25	12.3	171	23
40.1	16.5	180	183	6	32.0	165	32	21.6	150	32
28.0	23.0	180	185	3	39.0	163	22	54.3	169	21
26.0	17.0	160	170	3	84.0	178	36	70.0	175	26

those measured. A sample of the predicted results is given in Table 3 and the corresponding temperature and pressure profiles in Fig. 2. Table 4 shows a comparison between some measured and predicted values. The validity of this modeling exercise, however, can only be confirmed when it is successfully used for the prediction of other workers results. This, however, was not possible owing to the lack of adequate and comprehensive published data in the literature. When applied to other extruders of different sizes, including a commercial extruder (Creusot-Loire BC-92), the predicted results were generally in agreement with the plant measurements (barrel temperature and motor current). From the obtained results, the following points can be made.

(1) Uni-directional analysis of co-rotating twin screw extruders is realistic since good cross channel mixing is achieved by the relatively high screw speed, thus reducing product conductivity limitations.

(2) Food material (in this case, wheat A-starch) under extrusion conditions appeared to behave as a non-Newtonian fluid and its viscosity could be described reasonably well by the power law. The definition of shear rate was very important as it affected the physical and chemical changes in the product.

(3) The length of the melt pumping section was relatively short. In most cases of low moisture/fat concentration, it was only about one-two pitch length. This was in agreement with previous work carried out on a Creusot-Loire BC-72 extruder (Colona *et al.* 1983). The pressure gradient in the pumping section was much higher than that achieved by single screw extruders. Increasing the feed rate had no effect on the pressure gradient in the melt pumping zone but it increased the length of the filled section since a higher pressure is required behind the die to force the increased flow-rate through. Increasing the screw speed or the material viscosity (through reducing the moisture or fat content) produced however a higher pressure gradient in the pump section as demonstrated by Eq. 36 resulting in a shorter pump section. Equation 36 also shows that an increase in the screw diameter, a decrease in the flight depth and a decrease in the helex angle will also produce a higher pressure gradient and hence a shorter pump section.

(4) Under conditions of high viscosity and high operating speeds, the contribution of barrel heating was relatively small. This becomes smaller in commercial extruders since the throughput is roughly proportional to D^3 while the heat transfer area is proportional to D^2 only.

(5) The presence of a reverse element at the end of the screw shaft was essential to achieve relatively high product temperatures at moderate screw speeds. It also had significant effects on the product textural properties. In cooker twin screw extruders, it is normal to incorporate some form of screw restrictions before the die in order to lengthen the melt section

thus enabling increased mechanical energy input to the material. They can also be placed in other positions to achieve specific shear stress profiles or in some cases for depressurizing the barrel before a ventilation (or vacuum application) section.

(6) In order to account for all the heat supplied to the product, a product specific heat value of 2.7 kj/kg°C was assumed. This is relatively high for low moisture cereal products (Mohsenin 1980) which suggests that some heat was consumed as heat of melting/reaction. Similar findings were reported (Sahagun and Harper 1980) using a single screw extruder. At high viscosity the starch material undergoes a considerable degree of molecular breakdown. Measurement of its specific heat is unfortunately not possible under real extrusion conditions as the measuring methods (DSC and others) are limited to static sample conditions.

CONCLUSIONS

Co-rotating twin screw extrusion of food material was satisfactorily simulated. This was based on theoretical understanding and intuitive assumptions supported by experimental verification. Although food extrusion is a very complicated system, a uni-directional analysis proved very useful in the design and optimization of extruder operations. Predicting the effect and interaction of design parameters and operating variables provides considerable help in determining the direction in which the investigation should proceed in order to maximize or minimize a specified objective function. In cooker extruders, such variables affect directly the product physico/chemical and functional properties. Ideally therefore, such modeling exercise should be extended to incorporate a quantitative assessment of the product properties and how they can be influenced by the extruder design and operating conditions. Considerable basic research work needs to be done to identify in detail: (1) The mechanism of fluid flow and energy transfer and (2) the phase changes the food material is undergoing and their effect on its physical and chemical properties.

ACKNOWLEDGMENTS

The author wishes to thank: the Director of RHM Research Centre, Dr. J. Edelman, for allowing the publication of this manuscript; the Programme Manager Dr. G. L. Solomons; the Head of Process Development Dept., Mr. E. C. Pape and Dr. M. C. Jones of Aston University in Birmingham for encouragement and valuable discussions; Mr. J. Gourlay and Miss A. Horn for help with the experimental work; and Mrs. J. Wharton for her patience in typing the manuscript.

NOTATION

A	Surface area, m^2
a_1	Moisture coefficient of viscosity
a_2	Fat coefficient of viscosity
B	Width of the drilled cross channel in the reverse screw element, m
b	Temperature coefficient of viscosity $1/°C$
C_1	Geometry factory, m^3
C_2	Viscous heat dissipation factor, $°C/m$
C_3	Barrel/melt convection heat transfer factor, $°C/m$
C_4	Potential energy factor, $°C/m$
C_v	Specific heat $kj/m^3 \cdot °C$
c	General clearance width, m
D	Screw diameter, m
d	Die hole diameter, m
E	Motor energy, W
e	Screw flight tip width, m
F	Fat concentration, % of total weight
G	Depth of the drilled cross channel in the reverse screw element, m
H	Barrel heat supply or loss, W
h	Screw channel depth, m
I	Center to center distance between the two screw shafts, m
K_1	The reverse screw element conductance factor, m^4
K_2,K_3	Pressure profile factors for the pumping section and the reverse screw section respectively, N/m^3
K_4,K_5	Viscous heat dissipation factors for the pumping section and the reverse screw section respectively, $N \cdot m/s$
K_d	Die hole conductance, m^3
k	Thermal conductivity, $W/m \cdot °C$
L	Barrel length, m
l	Die plate hole length, m
M	Mass flow rate, kg/s
MC	Moisture concentration, % of total weight
m	No. of screw flight starts
m_1	No. of cross channels drilled in the reverse screw element
N	Screw speed, $1/s$
$n,n_1,$	Power low index
n_2,n_3	Power low index
P	Pressure, N/m^2
Q	Volumetric flowrate m^3/s
S	Specific energy consumption, $W \cdot s/kg$
T	Temperature, °C
U	Convection heat transfer coefficient $W/m^2 \cdot °C$
u	Relative material velocity in the clearance, m/s
V	Channel volume, m^3
v	Material velocity within the channel
x	Axial distance or coordinate, m
Z	Energy due to viscous heat dissipation, W
z	Coordinate parallel to the screw channel
α	Distance between the screw flight tip and the inside surface of the barrel, m
ϵ	Distance between the flight tip of one screw and the bottom channel of the other, m
σ	Distance between flights of opposite screws parallel to each other, m
υ	Screw filling ratio in the solid conveying section
μ	Viscosity, $N \cdot s/m^2$
γ	Shear rate, $1/s$
ϵ	Extruder efficiency factor
θ	Screw helix angle, radians

Subscripts

a	Air
b	Barrel
d	Die hole

Subscripts Continued

e	Equivalent	°	Initial or reference condition
f	Feed material	p	Pumping section
i	Inside barrel surface	r	Reverse screw section
m	Melt	s	Solid (powder)
o	Outside barrel surface	t,T	Total

REFERENCES

BIRD, R. B., STEWART, W. E. and LIGHTFOOT, E. N. 1960. *Transport Phenomena.* John Wiley & Son, Inc., New York.

BOOY, M. L. 1980. Polym. Eng. & Sci. *20*, (18), 1978. 1220.

BURKHARDT, K., HERMANN, H. and JAKOPIN, S. 1978. SPE ANTEC Technical Papers, Volume XXIV, Washington, DC.

CERVONE, N. W. and HARPER, J. M. 1978. J. Food Process Eng. *2*, 83.

CHEN, Y. C. J., LEWANDOWSKI, D. and IRWIN, W. E. 1978. J. Food Process Eng. *2*, 97.

COLONA, P., MELCION, J.-P., VERGNES, B. and MERCIER, C. 1973. J. Cereal Sci. *1*, 115.

DENSON, C. D. and HWANG, J. R. 1980. Polym. Eng. & Sci. *20*, (14), 965.

HARPER, J. M. 1981. *Extrusion of Food.* Vol. 1, CRC Press Inc.

HARRIOTT, P. 1959. Chem. Eng. Symp. Ser., *55* (29), 137.

JANSSEN, L. P. B. 1978. *Twin Screw Extrusion.* Elsevier Sci. Pub. Co.

JENSON, V. G. and JEFFREYS, G. V. 1977. *Mathematical Methods in Chemical Engineering.* Academic Press, New York.

MARTELLI, F. G. 1982. *Twin Screw Extruders: A Basic Understanding.* Van Nostrand, Reinhold, New York.

McKELEVEY, J. M. 1962. *Polymer Processing.* John Wiley & Sons, Inc., New York.

MOHSENIN, N. N. 1980. *Thermal Processing of Food and Agricultural Materials.* Gordon and Breach Science Publishers, Inc., New York.

OLKKO, J., HASSINEN, H., ANTILLA, J., POHJANPALO, H. and LINKO, P. 1980. *Food Process Engineering.* Vol. 1. Applied Sci. Publishers Ltd., London, England.

REMSEN, C. H. and CLARK, J. P. 1978. J. Food Process Eng. *2*, 39.

SAHAGUN, J. F. and HARPER, J. M. 1980. J. Food Process Eng. *3*, (4), 199.

SCHENKEL, G. 1966. *Plastic Extrusion, Technology and Theory.* Illiffe Books Ltd., London, England.

WYMAN, C. E. 1975. Polym. Eng. & Sci. *15* (8), 606.

SOLAR OSMOVAC-DEHYDRATION OF PAPAYA

J. H. MOY
and
M. J. L. KUO
Department of Food Science and Human Nutrition
University of Hawaii at Manoa
Honolulu, Hawaii 96822

Submitted for publication: September 29, 1980
Accepted for publication: April 6, 1981

ABSTRACT

A solar osmotic dryer was designed and constructed to test the utilization of solar energy in the two-step osmovac-dehydration of papaya. Drying rates measured in solar versus nonsolar osmotic dehydration experiments showed that solar osmotic drying had higher drying rates and sucrose uptake in the papaya samples (0.6 cm thick x 4 cm long x 2 cm wide) than in the nonsolar runs. In separate experiments, drying rates from solar vacuum-drying (as a second step of the osmovac-drying process) were about twice those of nonsolar vacuum-drying. Drying rates of both solar and nonsolar vacuum-drying reached the end of the constant-rate period in about 3 h. Sensory qualities of solar osmovac-dried papaya were comparable to those of vacuum-dried or solar osmotic-nonsolar vacuum-dried. These results suggest the possibility of drying rate increase and quality retention in utilizing solar energy in the osmovac-dehydration process.

INTRODUCTION

Osmovac-dehydration of foods is a two-step process involving the transfer of water molecules across a semipermeable membrane into a hypertonic surrounding followed by vacuum dehydration (Ponting *et al.* 1966; Farkas *et al.* 1969). The extent of dehydration by this technique depends on the nature of the membrane as well as the osmotic pressure created (Camirand *et al.* 1968). Ponting and his coworkers (1966) reported that fruits dried by osmosis had better flavor retention, less discoloration and minimized heat damage. Further drying is usually needed to bring the

Journal Series No. 2911 of the Hawaii Institute of Tropical Agriculture and Human Resources, University of Hawaii.

Journal of Food Engineering 8 (1985) 23-32.

remaining water content to a suitable level for storage stability. Higher dehydration rate can be achieved at higher temperature due to increased osmotic diffusion rate (Moy 1975).

Vacuum-drying as a second step is suitable for osmotically dehydrated fruit. Vacuum-drying rates are influenced by the heat input and the degree of vacuum.

According to Ponting and his coworkers (1966), osmovac-dehydration was less expensive and provided better flavor retention of the fruit than freeze-drying. The dried fruit pieces also had a very crisp, honeycomb-like texture excellent for eating as snacks or can be reconstituted and used as pie fillings.

Since thermal energy is required in the osmovac-dehydration process, solar energy may serve as an alternate source of heat to increase the drying rate. The objective of our work was to study the use of solar energy in the osmovac-dehydration of fruits using papaya as the main sample since it is a major fruit crop grown in Hawaii. The main emphasis was on system design, effect of solar energy on drying rates and product quality (Fig. 1).

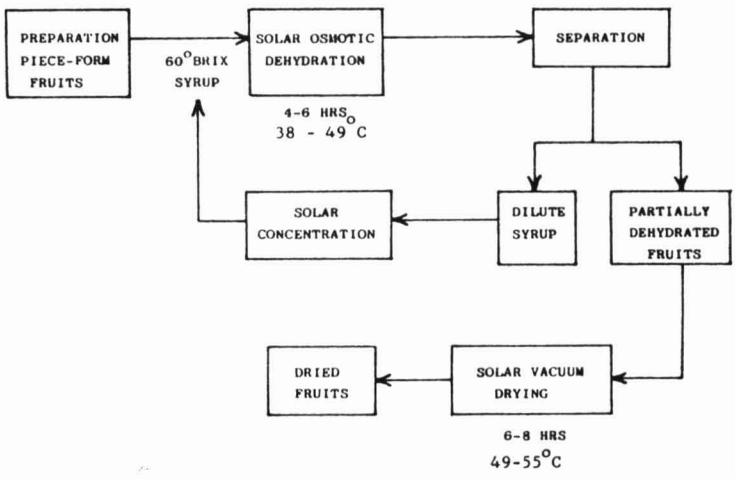

FIG. 1. SOLAR OSMOVAC-DEHYDRATION FOR PIECE-FORM FRUITS.

EXPERIMENTAL

Dryer Design and Construction

Solar Osmotic Dryer. Four 10 × 15 × 20 cm (approximately 2.5 liter) plexiglass (0.6 cm thick) vessels and four 9 × 13 × 18 cm stainless steel racks with slidable shelves (Fig. 2 and 3) were built. Two holes of 1.27 cm diameter were bored for connection to a bench type oscillating pump with a flow rate of about 36 liters/min (VWR, Bellville, Ohio). The stem of 10-cm long "selectapette" pipette tips (Clay Adams, Parsippany, New Jersey) was drilled with several holes of 0.16 cm diameter to distribute the syrup more uniformly in the syrup vessel.

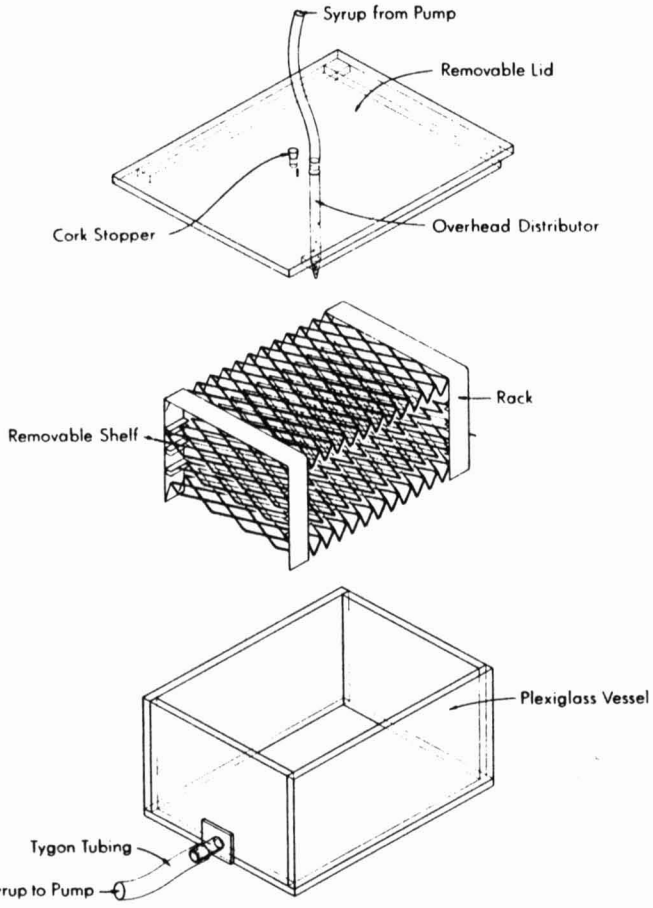

FIG. 2. VESSEL AND RACKS BUILT FOR SOLAR OSMOTIC DEHYDRATION OF PAPAYA SLICES.

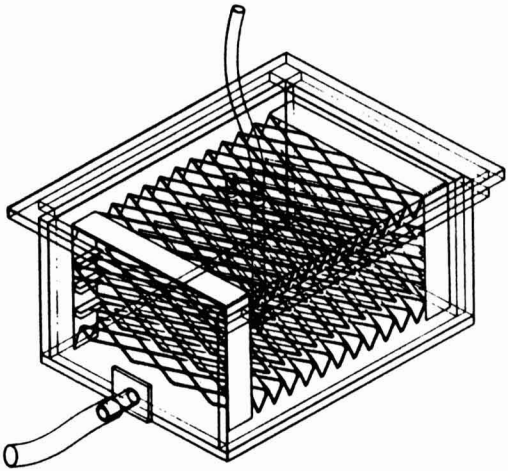

FIG. 3. VESSEL AND RACKS ASSEMBED FOR SOLAR OSMOTIC DEHYDRATION.

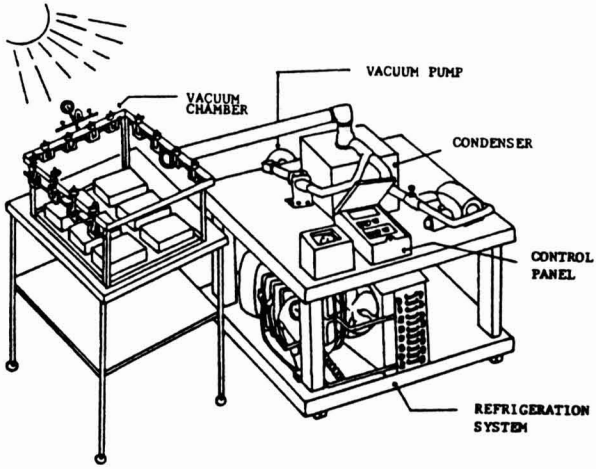

FIG. 4. COMPONENTS BUILT FOR SOLAR VACUUM-DRYING.

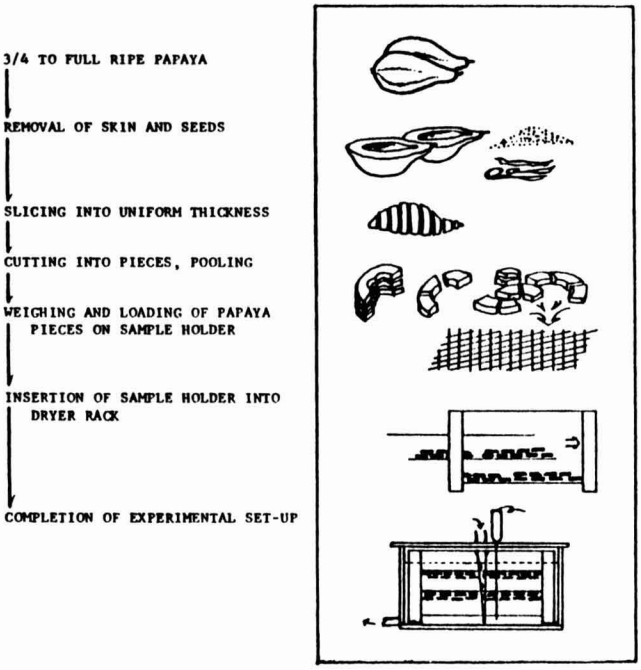

FIG. 5. PREPARATION OF PAPAYA SAMPLES FOR SOLAR OSMOTIC DEHYDRATION.

Solar Vacuum Dryer. A 56 × 56 × 25 cm plexiglass (3.8 cm thick) chamber and a portable condenser-vacuum unit were constructed (Fig. 4).

Drying Rates Measurements

Sample Preparation. Fresh papayas (3/4 to full ripe) were hand-peeled, sliced, and cut into pieces of 0.6 cm thick × 4 cm long × 2 cm wide (Fig. 5). Three hundred g of papaya were weighed, spread out equally onto two slidable shelves and then loaded into one rack. With 2100 g of 60° B_x sucrose syrup per vessel (syrup to fruit ratio: 7/1), the papaya pieces were completely submerged in the osmotic dryer.

Solar Versus Nonsolar Osmotic Drying. Drying rates were measured by the gravimetric method. Experiments were conducted in four osmotic vessels at the same time with or without exposure to the sun for eight h per run. Weight measurements were taken at the end of 1.5, 3, 4 and 5 h, respectively, by stopping one vessel at a time sequentially. At the end of

8 h, measurements were completed in all four vessels. To measure sample weight changes, papaya pieces were removed from the rack into a strainer, rinsed quickly with tap water, drained on absorbing paper and weighed. After weighing, 5 g of sample were removed for determination of soluble solids content. Syrup concentration was also measured. Temperatures of syrup were measured with copper-constantan thermocouples and recorded continuously on a Honeywell potentiometric recorder.

Solar Versus Nonsolar Vacuum Drying. Vacuum drying of solar osmotically dehydrated papaya were carried out in the solar vacuum dryer at 3.5 mm Hg. Weight measurements were taken at the end of 3, 5, 6 and 8 h for solar vacuum-dried samples and at the end of 1, 2, 3, 4, and 13 h for the nonsolar vacuum-dried samples. Temperatures at the geometric center of samples were measured with copper-constantan thermocouples and recorded continuously.

Quality of Solar Osmovac-Dehydrated Papaya

The quality of solar osmovac-dehydrated papaya was assessed by analyzing the ascorbic acid (AOVC Method 1966), texture and by a taste panel. Samples with different treatments (1) vacuum-drying; (2) solar osmovac-drying; and (3) solar osmotic- nonsolar vacuum-drying were compared. Data were analyzed by analysis of variance and Duncan's multiple range tests.

RESULTS AND DISCUSSION

Drying Rate and Sucrose Uptake

Solar Versus Nonsolar Osmotic Dehydration. Results from replicate experiments indicated that solar osmotic drying had higher rates as well as sucrose uptake in the samples, as expected. Figure 6 shows that as the temperature of the syrup rose sharply from 0 to 3 h, the sample moisture also decreased at the highest rate for solar osmotic dehydration. To reduce the sample moisture from about 90% to 70% (w/w), a nonsolar osmotic run required about 7.5 h whereas a solar osmotic run required only 5 h. Figure 7 shows that sucrose uptake was comparatively higher in the solar runs than in nonsolar osmotic runs. In general, higher syrup temperature resulted in higher drying rate and sucrose uptake.

Solar Vesus Nonsolar Vacuum-Drying. Results from solar vacuum-drying of solar osmotically dehydrated papaya showed that the drying

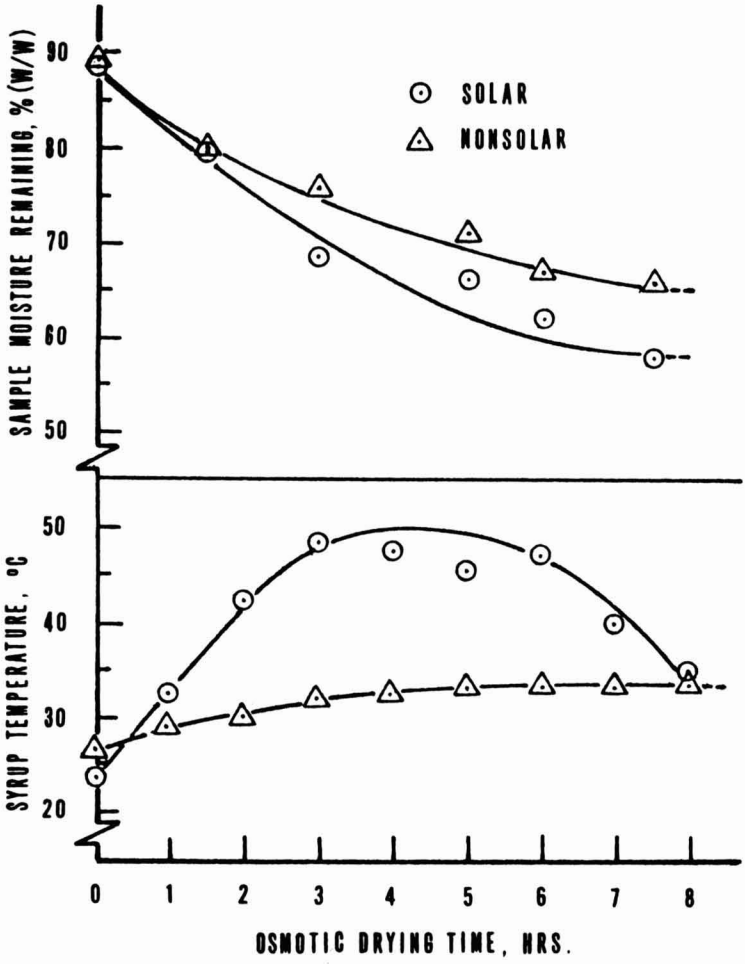

FIG. 6. DEHYDRATION RATES (TOP) AND SYRUP TEMPERATURES (BOTTOM) OF SOLAR VS. NONSOLAR OSMOTIC DEHYDRATION OF PAPAYA SAMPLES (0.6 CM THICK x 4 CM LONG x 2 CM WIDE)

rate was about twice as high as that of nonsolar vacuum-drying under the experimental conditions. Drying rates of both solar and nonsolar vacuum-drying reached the end of the constant-rate period in about 3 h as shown in Fig. 8. The moisture contents of the sample was reduced from about 58% to 18% (w/w) within 5 h in the solar runs.

Dried Fruit Quality

Results of sensory evaluation of three types of dried papaya slices by a trained taste panel of 12 are shown in Table 1. The color, flavor, texture and overall acceptability of vacuum dried, solar osmovac-dried, and solar

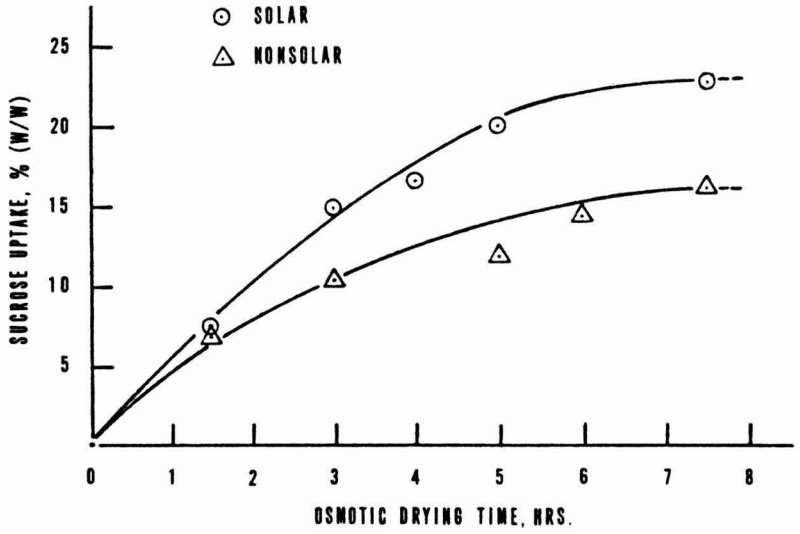

FIG. 7. AVERAGE SUCROSE UPTAKE (PERCENT, W/W) IN PAPAYA SLICES DURING SOLAR AND NONSOLAR OSMOTIC DEHYDRATION.

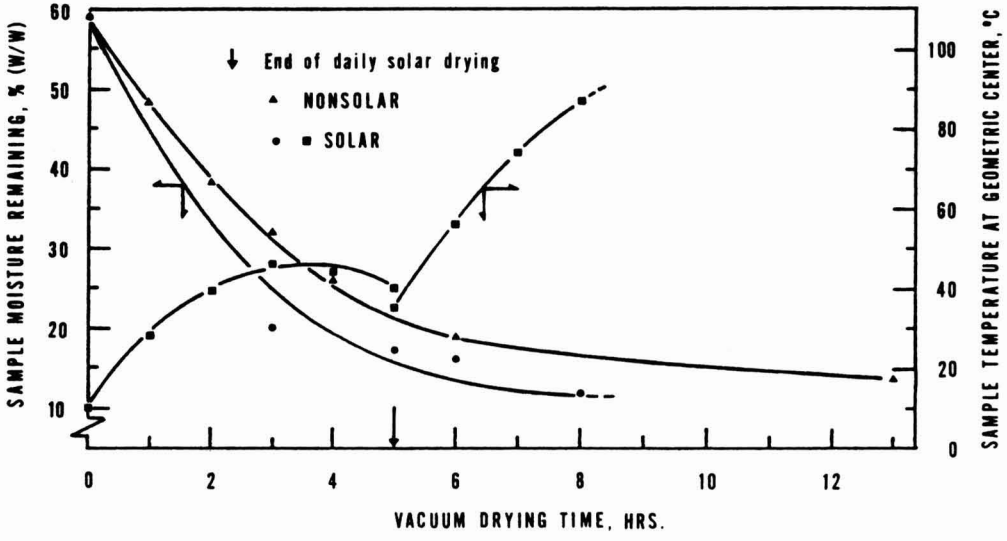

FIG. 8. DEHYDRATION RATES AND SAMPLE TEMPERATURES OF SOLAR VS. NONSOLAR VACUUM DEHYDRATION OF PAPAYA SLICES.

Table 1. Taste panel evaluation and ascorbic acid content of three types of dried papaya[a,b]

Quality	Vacuum Drying	Solar Osmovac	Solar Osmotic & Nonsolar Vacuum
Color	5.4	4.9	5.7
Flavor	4.6	5.6	5.6
Texture	3.6	3.8	4.4
Overall Acceptability	3.8	4.4	4.8
Ascorbic Acid, mg/100 g dry weight[c]	110	90	97

[a]Taste panel of 12; average of triplicate runs; hedonic scale of 7: 7 (like very much); 4 (neither like nor dislike); 1 (dislike very much).

[b]Data first analyzed by ANOVA for significance; further analyzed by Duncan's multiple range test. Numbers jointly underlined are not significantly different, otherwise significantly different at $p < 0.05$.

[c]Reference: fresh papaya 114 mg/100 g, all based on 100 gm dry weight.

osmotic-nonsolar vacuum-dried papaya slices were compared on a hedonic scale of 7 (Table 1). It is interesting to note that the color of the solar osmovac-dried papaya was not significantly different from that of vacuum-dried papaya, but both were scored significantly lower than the solar osmotic-nonsolar vacuum-dried samples ($p < 0.05$).

In flavor, the solar osmovac samples were comparable to that of solar osmotic-nonsolar vacuum-dried samples, and both were scored significantly ($p < 0.05$) higher than vacuum-dried samples.

In texture and overall acceptability, analysis of variance showed no signficant difference among the three types of dried samples.

A PEP Texture Tester (Houston, Texas) was used to measure the texture of the various samples. Unfortunately, the instrument did not function properly because of the relative toughness of the sample.

Table 1 also shows the ascorbic acid contents of the three dried papaya samples. As expected, the vacuum-dried samples retained 110 mg of

ascorbic acid per 100 gm of dry pulp, which was significantly ($p < 0.05$) different from the 90 and 97 mg/100 g of the solar osmovac and solar osmotic-nonsolar vacuum-dried samples, respectively. The ascorbic acid content from fresh papaya used in the experiment was 114 mg/100 g dry pulp.

CONCLUSION

The technology of utilizing solar energy for osmovac-drying of papaya was demonstrated. Drying rates in both the solar osmotic and vacuum-drying steps increased appreciably under the conditions investigated. Sensory qualities of solar osmovac-dried papaya (color, flavor, textures, overall acceptability) were comparable to those of samples that were vacuum dried or solar osmotic-nonsolar vacuum-dried. The results of drying rates and quality evaluation suggest that the solar osmovac-drying process could be quite feasible.

REFERENCES

AOVC. 1966. *Methods of Vitamin Assay.* 3rd Ed. Association of Vitamin Chemists, Inc. Interscience Pub., Inc. New York.

CAMIRAND, W. M., FORREY, R. R., POPPER, K., BOYLE, F. P. and STANLEY, W. L. 1968. Dehydration of membrane-coated foods by osmosis. J. Sci. Food Agric. *19*, 472.

FARKAS, D. F. and LAZAR, M. E. 1969. Osmotic dehydration of apple pieces. Food Technol. *23*(5), 90.

MOY, J. H. 1975. Res. Report to Int. Sugar Res. Foundation. Bethesda, MD.

PONTING, J. D., WATTERS, G. G., FOREY, R. R., JACKSON, R. and STANLEY, W. L. 1966. Osmotic dehydration of fruits. Food Technol. *20*(10), 125.

HEAT TRANSFER COEFFICIENTS TO NEWTONIAN LIQUIDS IN AXIALLY ROTATED CANS

CARLOS LUCIO SOULÉ[1]
and
RICHARD L. MERSON

Department of Food Science and Technology
Department of Agricultural Engineering
University of California
Davis, CA 95616

Submitted for publication: October 11, 1982
Accepted for publication: January 4, 1983

ABSTRACT

Overall heat transfer coefficients to water and silicone fluids in cans rotating in a steam retort were correlated by (Eq. A):

$$Nu_u = \frac{UD}{k} = 0.434\ Re^{0.571} Pr^{0.278} \left(\frac{L}{D}\right)^{0.356} \left(\frac{\mu_b}{\mu_w}\right)^{0.154} \qquad (A)$$

where the Reynolds number, $\rho ND^2/\mu$, based on the rotational speed of the can, was varied over the range $12 < Re < 44{,}000$, the Prandtl number $c_p\mu/k$ was tested between 2.2 and 2300, the can length to diameter ratio was varied over $1.11 < L/D < 1.61$, and the ratio of bulk to wall viscosities, μ_b/μ_w, was varied between 1.22 and 1.79. All fluid properties were evaluated at the arithmetic average of the initial and final temperatures of the can wall. Data for 106 trials were correlated with a multiple regression correlation coefficient of $R' = 0.916$. Internal film coefficients were about 7% higher than U values and can be calculated by $h = (1.07 \pm 0.04)\ U$.

INTRODUCTION

Although rotating canned foods in a steam environment is one of the most widely-used methods of sterilization, surprisingly little information

[1]Author Soulé received a fellowship from the Consejo Nacional de Investigaciones Cientificas y Tecnicas of Argentina to conduct this work. His permanent address is Instituto Nacional de Tecnologia Industrial, Centro de Investigaciones de Tecnologia Pesquera, Marcelo T. de Alvear 1168, 7600 Mar del Plata, Argentina

concerning heat transfer coefficients for this situation appears in the open literature. Quast and Siozawa (1974) made extensive measurements of heat transfer rates from steam to cans containing food materials or solutions of sugar or carboxymethylcellulose. Their data for overall heat transfer coefficients for sugar solutions can be correlated with a maximum error of ±33% (Merson *et al.* 1981) by (Eq. 1):

$$Nu_u = \frac{UD}{k} = 0.17\ Re^{0.52}Pr^{1/3}\ \left(\frac{L}{E}\right)^{1/3} \tag{1}$$

for $600 < Re < 250{,}000$. The Reynolds number here is defined as $Re = D_r(\pi DN)\rho/\mu$ where D_r is the diameter of the rollers turning the can. The term L/E accounts for variation in headspace but was not tested over a wide range. Based on tests with several liquid foods, Quast and Siozawa concluded that their sugar solution correlation could be used for other liquid foods of the same viscosity.

Naveh and Kopelman (1980) measured heat transfer rates, and visually inspected headspace bubble movement for a variety of rotational configurations, headspace values, and rotational speeds. They demonstrated that for high viscosity fluids, end-over-end rotation was more effective than axial rotation, heating gave higher heat transfer coefficients than cooling, and for promoting agitation the presence or absence of a headspace bubble was more important than its size. Average values for overall heat transfer coefficients during heating of 84° Brix, 70 D.E. glucose syrup in 105 × 122 mm cans rotating below 120 rpm ranged from about 30 W/m^2K (zero headspace, axial rotation) to 170 W/m^2K (10.7% headspace, end-over-end rotation).

Hotani and Mihori (1983), in a similar study, investigated mixing patterns and temperature distributions for both natural and forced convection in liquid products. They noted that low rotational speed (3 to 4 rpm) could be detrimental to rapid heat transfer because it interrupted natural convection patterns which are quite effective in liquid products. They also demonstrated that intermittent rotation was effective in promoting mixing by taking advantage of inertial turbulence.

Merson *et al.* (1981) reported heat transfer coefficients for a 60% sucrose solution in a 303 × 406 can axially rotating in a gas flame, simulating conditions for flame sterilization. Film coefficients from the inside surface to the liquid ranged from $h = 437\ W/m^2K$ at 59° C to $h = 500\ W/m^2K$ at 99° C and could be correlated by replacing the coefficient 0.17 in the Quast and Siozawa correlation by 0.37.

The studies presented in the following sections supplement the results of

previous investigators, extending the range of Re and Pr and including new dimensionless numbers based on theoretical considerations. For the experimental work, fluids with well-defined thermal properties were used, fluids whose properties are stable with repeated heating. Since the energy transport involved in heating canned foods is inherently unsteady state, the heat transfer coefficients reported in such tests are, in theory at least, average values over the temperature range of the can contents. To facilitate calculations, care was taken to create a temperature step function for the heating medium. This simulates the heating conditions in continuous rotary pressure or atmospheric cookers commonly used for sterilizing liquid products. The results could also be applied to rotary batch retorts or unconventional retorts where the ambient process temperature is constant and the retort coming-up time is short compared to the process time.

HEAT TRANSFER ANALYSIS

The ideal heat transfer analysis would be to solve the partial differential equations that describe the product motion and temperature distribution. Unfortunately, with the presence of headspace in the can, the liquid flow patterns are very complex during rotation and even numerical solution of the equations seems remote at the present time.

However, for rotating cans containing liquid foods and headspace gases, evidence exists that the temperature distribution within the liquid is quite uniform (Hotani and Mihori 1983; Merson *et al.* 1981). This indicates that there is good mixing within the fluid and that a film heat transfer model may be used. Defining a heat transfer coefficient h based on the entire surface area of the can, and using it in the macroscopic energy balance for the can, yields an equation which permits evaluation of h from experimental data (Eq. 2):

$$h = \frac{Q}{A(T_w - T)} = \frac{mc_p}{A(T_w - T)} \frac{dT}{dt} \qquad (2)$$

Defining h by Eq. 2 requires two major assumptions: (1) The total surface area of the can is the correct heat transfer area to use, and (2) a single heat transfer coefficient may be used over the entire heat transfer surface. In order to choose the correct area when headspace volumes are present, it is necessary to consider how the gas phase could affect the area for the heat transfer to the can contents. For still cans, in which the predominant mechanism for heat transfer is natural convection, the head-

space gases act as an insulation to the heat transmission, decreasing the transfer area with respect to the total area of the can. For example, if the can is oriented vertically with length L and headspace height E, the effective area for the heat transfer would be the bottom end plus the side wall from the bottom to a height equal to L minus E.

For agitating cans, one might assume that due to the headspace gases part of the total can area would not be in contact with the liquid. If this were true, then the transfer coefficients based on the total area would be expected to decrease as the headspace increased. However, experimental evidence suggests that the heat transfer coefficient in rotating cans actually increases with headspace, but only slightly. Approximate calculations made by Quast and Siozawa (1974) indicate that the time during which the top fraction of the can area is not in contact with the liquid contents is very short, and during this time the can wall stores heat which it transmits to the can contents when contact is resumed. Naveh and Kopelman (1980) indicate that the mere presence of a minimally-sized headspace, less than 2% of the can volume, markedly increases the heat transfer coefficient, because it promotes better internal agitation. Further enlargement of headspace volume further improves the heat transfer coefficient only slightly. From this evidence, it can be assumed that the total area of the can is effective for the heat transfer by forced convention.

The problem of which heat transfer coefficient to use over the can surface area A may be attacked as follows. Ignoring any effect of headspace gases, the rate of heat flow at the can walls is given by (Eq. 3):

$$Q = -\int_A (\mathbf{q} \cdot \mathbf{n}) dA \tag{3}$$

where $\mathbf{q}$ is given by the Fourier Law for conduction (Eq. 4):

$$\mathbf{q} = -k\nabla T \tag{4}$$

or, using the entire surface area, (Eq. 5):

$$Q = \int_0^L\int_0^{2\pi} k \left(\frac{\partial T}{\partial r}\right) \Big|_{r=R} R d\theta dz + \int_0^R\int_0^{2\pi} k \left(\frac{\partial T}{\partial z}\right) \Big|_{z=0} r d\theta dr$$

$$+ \int_0^R\int_0^{2\pi} k \frac{\partial T}{\partial z} \Big|_{z=L} r d\theta dr \tag{5}$$

Using Eq. 1 to define h employing the entire surface area, i.e., Eq. 6:

$$Q = h\left(\pi LD + \frac{\pi D^2}{2}\right)(T_w - T) \tag{6}$$

implies that k is spatially constant, that the temperature gradients are constant and equal

$$\frac{\partial T}{\partial r}\Big|_{r=R} = \frac{\partial T}{\partial z}\Big|_{z=0} = \frac{\partial T}{\partial z}\Big|_{z=L} \approx \frac{T_w - T}{\delta}$$

and $h = k/\delta$. For conduction heating products, Uno and Hayakawa (1980) have reported that the external surface heat transfer coefficients applicable to the top, bottom, and side surfaces of a cylindrical can are all different. Obviously, for a convection heating food, the heat fluxes from the top and bottom and from the side wall are different since the temperature gradient at each surface is a function of the geometry. Furthermore, along the surface of each of the three can walls, the heat fluxes are a function of position, since the radial and axial temperature gradients at the walls are a function of the respective spatial coordinates. For example, the interior boundary layer near the double seam is undoubtedly thicker than the boundary layer at the center of the side wall or can end. However, in spite of these difficulties, using Eq. 6 to define the heat transfer coefficient based on the total area of the can is the most convenient from the point of view of its practical application in thermal process calculations. If more detailed information were available concerning temperature gradients, Eq. 5 and 6 together could be used to predict h and provide the proper averaging of h over the entire surface area.

To determine the correlation variables which affect the experimental heat transfer coefficients, we set Eq. 5 and 6 equal, introduced dimensionless variables and derived that (Eq. 7):

$$Nu = Nu\left(t^*, Re, Pr, \frac{L}{D}\right) \tag{7}$$

where

$$Nu = hD/k, \qquad Re = \rho ND^2/\mu, \qquad Pr = \mu c_p/k$$

In arriving at Eq. 7, we made use of the functional dependence of temperature in the agitated can

$$T^* = T^*(r_i^*, t^*, Re, Pr)$$

derived using dimensional analysis (Soulé 1981) from the point equations (e.g., Bird *et al.* 1960), initial conditions, and boundary conditions for velocity, piezometric pressure, and temperature.

Equation 7 establishes the dimensionless groups that have to be considered in the planning and interpretation of experiments. Both Eq. 7 and Eq. 2 assume: (1) constant physical properties, (2) ideal mixing, (3) Newtonian rheological behavior, (4) negligible viscous dissipation effect and (5) single phase system.

The most serious assumption of the five listed above is that related to the constancy of physical properties. If the temperature difference between the can surface and the contents is considerable, as in the case of the higher temperature sterilization of non-acid or low-acid foods, viscosity variations could be important; if so, they could be taken into account by including a new group, μ_b/μ_w, where μ_b is the viscosity at some average value of the bulk temperature, and μ_w the viscosity at the wall temperature.

Hence, the form of the correlations of the Nusselt number for liquid canned foods will be (Eq. 8):

$$Nu = Nu(t^*, Re, Pr, \frac{L}{D}, \frac{\mu_b}{\mu_w}) \tag{8}$$

The same analysis could be made for the overall heat transfer coefficient U, and Eq. 2 to 8 would be valid simply by replacing in them h by U, T_w by T_s and Nu by Nu_u, where

$$Nu_u = \frac{UD}{k}$$

If the fluid is non-Newtonian but its flow behavior index is close to unity, as with many food products such as single strength tomato juice or fruit juices, Eq. 7 will be approximately valid by replacing the Newtonian viscosity μ by the apparent viscosity η, defined as the ratio of the shear stress to the shear rate at each rotational speed.

EXPERIMENTS

The experimental equipment was an adaptation of the single can process simulator described by Leonard *et al.* (1975). This device consisted of a stainless steel, sheet metal chamber with connections for saturated atmospheric steam inlet and condensate outlet. Two sets of rollers, with variable speed drive in the range 0-150 rpm, rotated the can in place at any desired speed.

The steam temperature in the chamber near the can was measured with a standard copper-constantan thermocouple. To determine the can surface temperature, a fine copper-constantan thermocouple was soldered onto the inside cylindrical wall at the midplane. In-can fluid temperatures were measured at the geometric center by mounting a CNL needle type, Ecklund copper constantan thermocouple (O. F. Ecklund Custom Thermocouples Incorporated, Cape Coral, Florida) through one end of each can.

The two inside thermocouples of the rotating can were connected to the outside through surface-mounting, locking female connectors (Model S-32) and rotary contactors (Model S-28, O. F. Ecklund Custom Thermocouples Incorporated, Cape Coral, Florida) at both ends of the can. The signals of these thermocouples were digitized, converted from mV to °C, and printed at 4 s intervals on paper tape using a data acquisition sytem (Esterline Angus PD 2064, Model No. 101, "Data Logger").

Distilled water and silicone oils (Dow Corning 200 fluids) of four different viscosities (1.5 cs, 20 cs, 50 cs and 300 cs at 77° F) were used as model fluids. The values for physical properties of water were taken from Batchelor (1967). The data for silicone fluids were taken from Technical Bulletin No. 22-069d-76 (Dow Corning Corporation, Midland, Michigan).

The cans used in the experiments were 303 × 406, 401 × 411 and 404 × 700, where L/D ratios were 1.32, 1.11 and 1.61, respectively. The head space height was 1.0 cm and the closing vacuum was 20 in. of Hg as is usual in liquid canned food processes.

One hundred six experiments were made and each process condition was repeated at least twice. The can weight was measured before and after each trial, and when it changed during the process, because of leakage through thermocouple connectors, the results were discarded. Also, results were discarded if the rotational speed changed between the start and the end of the experiment, as a consequence of being slowed down by the thermocouple rotary contactors.

RESULTS AND DISCUSSION

One way to evaluate the heat transfer coefficients from experimental data using Eq. 2 is to determine the slope of the heating curve by some approximate method, e.g., finite differences. With this approach, however, a small error in the determination of T results in a large error of $dT/dt \approx \Delta T/\Delta t$ if the numerator is small, a situation that occurs for the most viscous fluids.

An alternative way to evaluate h is by a simple integration of Eq. 1, which yields (Eq. 9 or 10):

$$h = \frac{mc_p}{At} \ln \frac{T_w - T_i}{T_w - T} \tag{9}$$

or

$$U = \frac{mc_p}{At} \ln \frac{T_s - T_i}{T_s - T} \tag{10}$$

Equations 9 and 10 are valid if m, c_p, A, h, U, T_w and T_s are constants and if the initial temperature of the product is uniform. To consider mc_p/A as a constant is a very good approximation in systems such as those studied here. It is easy to maintain T_s constant after the chamber come-up time, and if the come-up time is very short with respect to the overall process time, it is a very good approximation to consider T_s constant throughout the process. The small size of the chamber, and the availability of a good steam flow in the experimental equipment made it possible to limit the come-up time to only a few seconds. Moreover, taking advantage of the temperature uniformity at every time, as a consequence of the agitation, the temperature of the product when the chamber reaches the process temperature can be taken as the initial temperature and the process can be considered to start at this time. In this way, the steam temperature can be exactly simulated by a step function.

Thus, the only requirement for Eq. 10 to be valid is for U to be independent of time. For this case, the slope of $\ln\{(T_s - T_i)/(T_s - T)\}$

versus t would give information about the heat transfer coefficient and (Eq. 11):

$$U = \frac{m\, c_p}{A} \cdot \text{slope} \tag{11}$$

The linearity of $\ln\{(T_s - T_i)/(T_s - T)\}$ versus time would have to be checked and high values of the linear regression coefficients would indicate that Eq. 11 could be used.

With respect to the internal heat transfer coefficient, Eq. 9 would be valid only if T_w were constant (besides the previous considerations). This is not actually true but Eq. 9 could be considered as an approximate integral of Eq. 1 if

$$\frac{dT_w}{dt} \ll \frac{dT}{dt}$$

This inequality is satisfied in steam retorts where the internal heat transfer resistance is controlling the process. The heat transfer resistance of the thin metallic walls of cans and the condensing steam is very small compared to that of the liquid. Thus, the internal heat transfer coefficients could be calculated from the slope of $\ln\{(T_w - T_i)/(T_w - T)\}$ versus time, as follows, (Eq. 12):

$$h = \frac{m\, c_p}{A} \cdot \text{slope} \tag{12}$$

if linearity is first verified.

Linearity of the logarithmic heating curves was checked for each trial by calculating linear regression coefficients. The internal and the overall heat transfer coefficients were calculated from Eq. 12 and 11, respectively. The results are recorded elsewhere (Soule 1981) together with the calculated Nusselt, Reynolds and Prandtl numbers, the μ_b/μ_w ratio and the number of points taken in each linear regression.

The fluid physical property values used in the determination of the dimensionless groups were evaluated at the average bulk temperature betwen the start and the end of the process, except μ_w, which was evaluated at the time-averaged temperature of the can wall. Bulk temperature

increases between the start and end of the processes were in the range 40-80° C. In each calculation, the start of the process was taken as the time at which the chamber reached the process temperature, and the process was ended when the temperature difference between the fluid and the can wall reached 5° C. Large differences between the wall temperature and the bulk temperature were chosen in the experiments to include conditions for most conventional processes, and also to minimize the error in the calculations of the heat transfer coefficients. A small error in the determination of T results in a large change of $(T_w - T_i)/(T_w - T)$ if T is close to T_w.

High values of the correlation coefficients were obtained for linear regressions for both $\ln\{(T_s - T_i)/(T_s - T)\}$ versus t and $\ln\{(T_w - T_i)/(T_w - T)\}$ versus t (usually higher than 0.99) indicating that the functional dependence of h with time is not significant, and therefore Eq. 9 and 10 can be used. The calculated heat transfer coefficients were very reproducible (usually within ±2%) for experiments run under the same conditions (e.g., same can size, same fluid and same rotational speed).

A correlation for the Nu_u was obtained by postulating the following model according to Eq. 8 (Eq. 13):

$$Nu_u = a\, Re^{b_1}\, Pr^{b_2} \left(\frac{L}{D}\right)^{b_3} \left(\frac{\mu_b}{\mu_w}\right)^{b_4} \tag{13}$$

The coefficient a and the exponents b_i were obtained by a multiple linear regression model after taking logarithms of both sides of Eq. (13), yielding (Eq. 14):

$$Nu_u = 0.434\, Re^{0.571}\, Pr^{0.278} \left(\frac{L}{D}\right)^{0.356} \left(\frac{\mu_b}{\mu_w}\right)^{0.154} \tag{14}$$

The corresponding multiple correlation coefficient was $R' = 0.916$.

An equation similar to Eq. 14 could be developed to correlate the internal heat transfer coefficient. However, since the heat transfer resistances of the can and steam side were constant under our experimental conditions (and under most practical situations), each h value differs from the corresponding U value simply by a constant. The experimental difference between h and U expressed as a percentage of h is (Eq. 15):

$$\frac{h-U}{h} \times 100 = 6.41 \pm 3.63 \tag{15}$$

where 6.41 was the mean for all the available data and 3.63 the standard deviation from the mean. Solving for h gives a more convenient form (Eq. 16):

$$h = (1.07 \pm 0.04)\, U \tag{16}$$

which can be used to calculate h using U values from the Nu_u correlation in Eq. 14.

In Fig. 1, the calculated values for all the experimental points considered in the regression analysis are shown, together with Eq. 14. The correlation fit is good for most of the experimental points, with a larger dispersion of values for the lower Reynolds numbers than for the higher ones. At low Reynolds number, there is less assurance of complete mixing and, in fact, one would expect some free convection to occur; in this case the Grashof number would need to be included in the correlation.

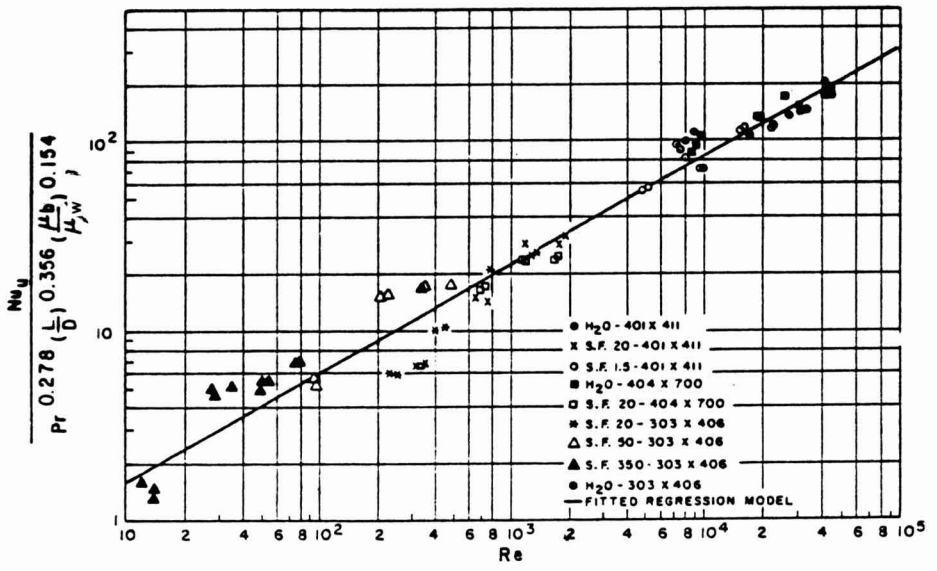

FIG. 1. CORRELATION FOR HEAT TRANSFER TO AXIALLY ROTATED CANS.

The ranges of Reynolds number, Prandtl number and temperature considered in the correlation are wide enough to cover most practical situations in conventional processes for liquid canned foods. Also, the L/D ratios tested, in spite of covering a small range, include the values for

most can sizes used in liquid food canning.

Limited calculations for typical processing conditions have shown that Eq. 1 and 14 give results of the same order of magnitude with Eq. 14 giving higher values and a stronger dependence on can rotation. For example, for heating a 60% sucrose solution in a 303 × 406 can from 95 to 121°C in 121°C steam (outside the temperature range of both correlations), the ratio of U calculated from Eq. 14 to U from Eq. 1 was 1.08 at 1 RPM and 1.21 at 10 rpm. Similarly, for water heated from 38 to 116°C, the same ratio was 1.38 at 1 rpm and 1.56 at 10 rpm. Recent work (Peralta Rodriquez and Merson 1983) has shown both equations to be useful when the properties of the liquids are known and the Reynolds number can be determined.

CONCLUSIONS

A correlation for the overall heat transfer coefficient in rotating cans was found using water and silicone oils as model fluids and steam as the heating medium:

$$Nu_u = 0.434\, Re^{0.571} Pr^{0.278} \left(\frac{L}{D}\right)^{0.356} \left(\frac{\mu_b}{\mu_w}\right)^{0.154}$$

for the following ranges of dimensionless groups:

$$12 < Re < 44{,}000$$

$$2.2 < Pr < 2{,}300$$

$$1.11 < \frac{L}{D} < 1.61$$

$$1.22 < \frac{\mu_b}{\mu_w} < 1.79$$

The internal heat transfer coefficient can also be estimated from this correlation by using the additional formula

$$h = (1.07 \pm 0.04)U$$

NOMENCLATURE

a	coefficient in the heat transfer model
A	total area of cylindrical can
b_1,b_2,b_3,b_4	exponents in the heat transfer model for Re, Pr, (L/D), and μ_b/μ_w, respectively
c_p	specific heat capacity at constant pressure per unit mass
D	can diameter
D_r	diameter of rollers turning the can
E	headspace height with can vertical
h	internal heat transfer coefficient
k	thermal conductivity of the fluid
L	can length
m	mass of fluid
$\mathbf{n}$	area unit vector
N	rotational speed
$\mathbf{q}$	local heat flux
Q	heat flow rate
r	radial coordinate
r_i^*	dimensionless spatial coordinates
R	can radius
R'	multiple correlation coefficient
S	surface area
t	time
t^*	dimensionless time (tN)
T	bulk temperature
T^*	dimensionless bulk temperature $[(T_w-T_i)/(T_w-T)$ for internal heat transfer calculations and $(T_s-T_i)/(T_s-T)$ for overall heat transfer calculations]
T_i	bulk temperature at the start of the process
T_s	steam temperature
T_w	can wall temperature
U	overall heat transfer coefficient
z	axial coordinate
δ	thickness of heat transfer boundary layer near interior can surfaces
ΔT	driving force for the heat transfer $[(T_w-T)$ for internal heat transfer calculations and (T_s-T) for overall heat transfer calculations]
∇T	temperature gradient
η	apparent fluid viscosity
ρ	fluid density
θ	polar coordinate
μ	absolute fluid viscosity
μ_b	fluid viscosity evaluated at the average bulk temperature between the start and the end of the process
μ_w	fluid viscosity evaluated at the average temperature of can wall between the start and the end of the process
Nu	Nusselt number based on h (hD/k)
Nu_u	Nusselt number based on U (UD/k)
Pr	Prandtl number ($c_p\mu/k$)
Re	Reynolds number ($\rho ND^2/\mu$)

REFERENCES

BATCHELOR, G. K. 1967. *An Introduction to Fluid Dynamics,* pp. 596-597, Cambridge Univ. Press, Cambridge, Mass.

BIRD, R. B., STEWART, W. E. and LIGHTFOOT, E. N. 1960. *Transport Phenomena*, p. 319, John Wiley & Sons, New York.

HOTANI, S. and MIHORI, T. 1983. Some thermal engineering aspects on the rotation method in sterilization, p. 121-129. In *Heat Sterilization of Foods, (K. I. Hayakawa and T. Motohito, eds.), Koseisha-Koseikaku Publishing Co., Tokyo.*

LEONARD, S. J., MERSON, R. L., MARSH, G. L., YORK, G. K., HEIL, J. R. and WOLCOTT, T. 1975. Flame sterilization of canned foods: An overview. J. Food Sci. *40*, 246-249.

MERSON, R. L., LEONARD, S. J., MEJIA, E. and HEIL, J. 1981. Temperature distributions and liquid-side heat transfer coefficients in model liquid foods in cans undergoing flame sterilization heating. J. Food Process Engineering. *4*, 85-98.

NAVEH, D. and KOPELMAN, I. J. 1980. Effects of some processing parameters on the heat transfer coefficients in a rotating autoclave. J. Food Processing and Preservation *4*, 67-77.

PERALTA RODRIGUEZ, R. D. and MERSON, R. L. 1983. Experimental verification of a heat transfer model for simulated liquid foods undergoing flame sterilization. J. Food Sci. *48*, 726-733.

QUAST, D. G. and SIOZAWA, Y. Y. 1974. Heat transfer rates during heating of axially rotated cans. Proc. IV Int. Congress Food Sci. and Technol. Vol. IV, 458-468.

SOULÉ, C. L. 1981. Internal Heat Transfer Coefficients in Liquid Canned Foods. M. S. Thesis. University of California, Davis, CA 95616.

UNO, J. I. and HAYAKAWA, K. I. 1980. Correction factor of come-up heating based on critical point in a cylindrical can of heat conduction food. J. Food Sci. *45*, 853-859.

CORRELATIONS FOR THE CONSISTENCY COEFFICIENTS OF APRICOT AND PEAR PUREES

DR. COSKAN ILICALI

Ege University
Department of Food Engineering
Izmir, Turkey

Submitted for publication: December 21, 1984
Accepted for publication: April 2, 1985

ABSTRACT

Two correlations for the consistency coefficients of apricot and pear purees have been developed. The consistency coefficient for the apricot puree within the given experimental range can be represented as $K = 3.7 \times 10^{-6} e^{1500/T}(\%TS)^{3.5}$ *and for the pear puree,* $K = 3.1 \times 10^{-6} e^{1450/T}(\%TS)^{3}$. *Experimental values obtained from the literature are compared with the predictions obtained using the above equations. The level of agreement is generally satisfactory. It is recommended that the consistency coefficients for fruit purees be determined at known dissolved solids and insoluble solids content.*

INTRODUCTION

In process engineering, the viscosity or the consistency of a fluid is an important property. This property is used widely in designing fluid handling and heat transfer equipments. In food engineering, most of the fluid foods are solid-liquid mixtures whose consistencies differ widely depending on the nature of the mixture.

Fruit purees and concentrates can be represented by the power equation of the form (Eq. 1):

$$Z = K\alpha^n \tag{1}$$

where Z is the shear stress, Pa.
α is the shear rate, s^{-1}
K is the consistency coefficient, Pa $\times$ s^n
n is the flow behavior index, dimensionless

Journal of Food Engineering 8 (1985) 47-51.

K and n values for some fruit purees can be found in the literature (Charm 1978; Harper 1960; Heldman 1981; Holdsworth 1971; Saravacos 1968; Watson 1968). The flow behavior indices reported by different authors agree closely with each other. These indices are nearly independent from the total solid content and temperature within the reported experimental range. However, the consistency coefficient K is a strong function of temperature and concentration of solids in the puree.

The purpose of this paper is to suggest approximate correlations giving the consistency coefficients of apricot and pear purees as a function of temperature and the total solid content.

MATERIALS AND METHODS

An equation of the following form is assumed for the dependence of the consistency coefficient on temperature and the solid content (Eq. 2):

$$K = \alpha_o e^{E_a/RT}(\%TS)^c \qquad (2)$$

where α_o is the consistency constant, Pa $\times$ s^n
E_a is the activation energy, J/mol
R is the gas constant, J/mol$\times$K
%TS is the percent total solids
c is a dimensionless constant.

If the assumed form is correct, the plot lnK versus ln(%TS) will give a straight line at constant temperature. Determination of the activation energy for flow can be done in a similar manner by plotting the natural logarithm of the consistency coefficient against the reciprocal of the absolute temperature at constant percent total solid content.

RESULTS AND DISCUSSION

Figure 1 shows the plot lnK versus ln(%TS) for apricot and pear purees. Holdsworth's (1971) data are used. As can be seen, a better fit is obtained for the pear puree. The data points for 32° C and 82° C can be represented as two parallel straight lines. Similarly, the data points for the apricot puree, although the fit is poorer, can be represented as two parallel lines for 4.5° C and 60° C. Activation energy for flow can be estimated if it is assumed that the natural logarithm of the consistency coefficient K is a linear function of the reciprocal of the absolute temperature, which is the case for Newtonian fluids.

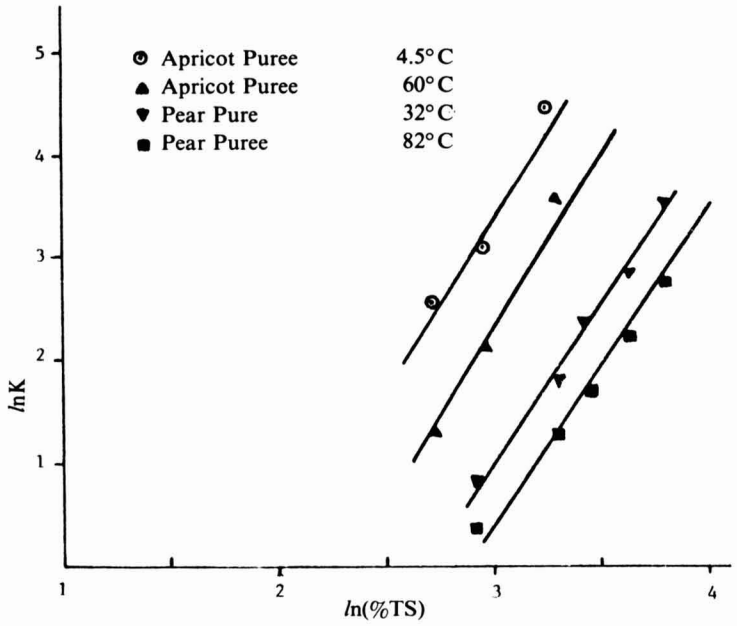

FIG. 1. THE DEPENDENCE OF THE CONSISTENCY INDEX ON THE SOLID CONTENT FOR APRICOT AND PEAR PUREES, (Holdsworth, 1971)

The resulting equations are (Eq. 3 and 4):

$$K, \text{Pa}\times s^n = 3.7 \times 10^{-6} e^{1500/T} (\%\text{TS})^{3.5} \text{ Apricot puree} \quad (3)$$

$$K, \text{Pa}\times s^n = 3.1 \times 10^{-6} e^{1450/T} (\%\text{TS})^{3} \text{ Pear puree} \quad (4)$$

In Table 1, the predicted consistency coefficients are compared with the data obtained from the literature.

As can be observed, the fit between the experimental values of Holdsworth and the predicted values is quite satisfactory for the pear puree. For the apricot puree, the data of Holdsworth (1971) can be predicted within approximately 25% accuracy. Some of the other predictions are poor. The consistency coefficient for the apricot puree at 21°C with a total solid content of 17.7% is reported by Harper (1960) as 5.4 Pa$\times s^n$, whereas the predicted consistency coefficient is 14.2 Pa$\times s^n$. However, for similar experimental conditions, the consistency coefficient for the apricot puree reported by Watson (1968) is 20 Pa$\times s^n$. The difference between such values may be due

Table 1. Comparison of the predicted consistency coefficients with experimental values for apricot and pear purees.

Temp., °C	%TS	Experimental K, Pa.s^n	Predicted K, Pa.s^n	Reference
Apricot purees and concentrates				
21	17.7	5.4	14.2	Harper(1960)
25	19	20	17.0	Watson(1968)
27	13.8	7.2	5.4	Saravacos(1968)
25	26	67	50.9	Watson(1968)
4.5	15.4	13	11.8	Holdsworth(1971)
4.5	19	22	24.7	Holdsworth(1971)
4.5	26	86	73.9	Holdsworth(1971)
60	15.4	3.8	4.8	Holdsworth(1971)
60	19	8.8	10	Holdsworth(1971)
60	26	40	30	Holdsworth(1971)
Pear purees and concentrates				
27	15.2	4.25	1.4	Harper(1960)
32	18.31	2.25	2.4	Harper and Leberman(1964)
32	45.75	35.5	36.9	Harper and Leberman(1964)
27	14.6	5.3	1.2	Saravacos(1968)
32	18.3	2.25	2.2	Holdsworth(1971)
32	26.1	6.2	6.3	Holdsworth(1971)
32	31.0	10.9	10.6	Holdsworth(1971)
32	37.2	17.0	18.3	Holdsworth(1971)
32	45.7	35.5	34.0	Holdsworth(1971)
82	18.3	1.41	1.1	Holdsworth(1971)
82	26.1	3.6	3.2	Holdsworth(1971)
82	31.0	5.6	5.4	Holdsworth(1971)
82	37.2	9.4	9.4	Holdsworth(1971)
82	45.7	16.0	17.4	Holdsworth(1971)

to the definition of "the total solid content" being not precise. Total solid content inludes the dissolved solids and the insoluble solids. Fruit purees having the same total solid content but with different ratios of dissolved solids to insoluble solids will necessarily have different consistency

coefficients. Therefore, the correlations proposed in this paper can be considered as approximations to the true values.

Experimental consistency coefficient values for fruit purees of known dissolved solids content and insoluble solids content must be available for the development of correlations of more general and accurate character. It is believed that such an approach may show the reason of inconsistency between experimental values of consistency coefficients having similar total solids content.

REFERENCES

CHARM, S. E. 1978. *Fundamentals of Food Engineering.* 3rd Ed. AVI Publishing Co., Inc., Westport, Connecticut.

HARPER, J. C. 1960. Viscometric behavior in relation to evaporation of fruit purees. Food Technol. *14*, 557.

HARPER, J. C. and LEBERMAN, K. W. 1964. Rheological behavior of pear purees. Proc. 1st. Intern. Congr. Food Sci. and Technol. 719-728.

HELDMAN, D. R. and SINGH, R. P. 1981. *Food Process Engineering.* 2nd Ed. AVI Publishing Co., Inc., Westport, Connecticut.

HOLDSWORTH, S. D. 1971. Applicability of rheological models to the interpretation of flow and processing behavior of fluid food products. J. Texture Studies *2*, 393-418.

SARAVACOS, G. D. 1968. Tube viscometry of fruit purees and juices. Food Technol. *22*(12), 1585-1588.

WATSON, E. L. 1968. Rheological behavior of apricot purees and concentrates. Cand. Agri. Engr. *10*(1), 8-12.

JFS ABSTRACTS

Chitosan Membranes for Reverse Osmosis Application. (1984) T. Yang, R. R. Zall. J. Food Sci. *49*, 91-93.

Alkali resistant reverse osmosis membranes were fabricated by spreading solutions of chitosan, a poly-N-acetyl glucosamine, in 2.0% acetic acid on a glass plate. The membrane had a flux rate of 1.67 x 10^{-3} $cm^3/cm^2/sec$ and a salt rejection capability of 78.8% with 0.2% NaCl at 680 psi. Addition of 40% polyethylene glycol to the membrane casting solution increased permeability, while 10% chloromethyl oxirane improved durability of the membranes.

Flow Behavior of Liquid Whole Egg During Thermal Treatments. (1984) M. Hamid-Samimi, K. R. Swartzel, H. R. Ball, Jr., J. Food Sci. *49*, 132-136.

Costs of handling and loss of functional properties of frozen liquid whole egg (LWE) has stimulated interest in a refrigerated product. To maintain adequate shelf life at refrigeration temperatures a heat treatment more severe than normal pasteurization may be needed. To establish limits for the thermal treatment and to prevent possible damage to the pasteurization system due to coagulation of the product, flow properties of LWE during pasteurization were investigated. Utilizing a cone and plate viscometer, egg viscosity was determined at shear rates between 1.15 and 450 sec^{-1}. Test temperatures varied from 20-75° C and heat treatment durations ranged from 0.5-10 min. Percent protein denaturation for each treatment was also determined and correlated to the flow properties. Above 60° C viscosities were shear rate dependent while below this temperature flow properties were approximately Newtonian. Mathematical expressions were developed for viscosity as a function of time, temperature and shear rate.

Modeling the Thermal Conductivity of Cooked Meat. (1984) M. G. R. Perez, Covelo. J. Food Sci. *49*, 152-156.

The thermal conductivity of cooked meat under different thermal treatments is measured and a mathematical model for its prediction is developed. Apparent and real densities, thermal conductivity and water content were evaluated on the cooked samples. The thermal conductivity showed good correlation with the water content. Values were found to be independent of the thermal history during cooking. Experimental results showed a good agreement with the proposed mathematical model that considers meat as composed by air and water spheres distributed over a matrix of dry fiber. Values for the parameters involved are provided, as well as expressions for the shrinkage of samples taking into account the incorporation of air during cooking.

Supercritical Fluid Extraction of Dry-Milled Corn Germ with Carbon Dioxide. (1984) D. D. Christianson, J. P. Friedrich, G. R. List, K. Warner, E. B. Bagley, A. C. Stringfellow, G. E. Inglett. J. Food Sci. *49*, 229-239 + 272.

Dry-milled corn germ was extracted with supercritical carbon dioxide (SC-CO_2) at 5,000-8,000 psi and 50° C, CO_2-extracted oil was lower in free fatty acids and refining

loss, and was lighter in color when compared with a commercial expeller-milled crude oil. Total unsaponifiable and tocopherol contents were similar for both oil types. The defatted, highly friable flour has a shelf-stable moisture content of 2-3% and good flavor quality. The flour contains 20% protein with good amino acid balance, meeting FAO specifications for food protein supplements. High pressure SC-CO_2 extraction also denatures the proteins, including oxidative enzymes. Peroxidase activity is reduced tenfold in SC-CO_2-extracted flour when compared with hexane-extracted flours. Storage tests for 5 wk at 38° C and for 2 months at 25° C show that flavor quality of untoasted SC-CO_2-defatted germ flour is maintained even under these extreme conditions.

Estimation of Microbial Populations in Frozen Concentrated Orange Juice Using Automated Impedance Measurements. (1984) J. L. Weihe, S. L. Seibt, W. S. Hatcher. J. Food Sci. *49*, 243-245.

Automated impedance measurements were used to classify samples of frozen concentrated orange juice as acceptable ($< 10^4$ CFU/ml) or unacceptable ($> 10^4$ CFU/ml). Calibration curves relating initial microbial concentration to impedance detection time were generated for several orange juice isolates. Cut-off times of 10.2 hr for bacteria and 15.8 hr for yeasts were adopted. More than 96% of 468 retail samples were correctly classified using automated impedance measurements. This technique has several advantages over other automated systems, including lower cost and reduced demand for technician time, and it provides reliable results much quicker than does the agar plate count.

Finite Element Analysis of Non-Linear Water Diffusion During Rice Soaking. (1984) T. Y. Zhang, A. S. Bakshi, R. J. Gustafson, D. B. Lund. J. Food Sci. *49*, 246-250 + 277.

The formulation of a finite element model is described that could be used to analyze water diffusion during rice soaking with concentration dependent diffusivity and change in the size of rice. The rice is divided into 135 elements and moisture distribution with time is calculated. Knowing the moisture absorbed by each element, the nodal displacements are obtained by minimizing the potential energy of the system. Average mass diffusivity of milled rice decreased from 6.4×10^{-7} to 3.0×10^{-7} m^2/hr as the moisture content increased from 13 to 50%. The density and concentration dependent mass diffusivity model adequately described experimental data.

Effect of Ultra High Temperature Processing and Storage Conditions on Rates of Sedimentation and Fat Separation of Aseptically Packaged Milk. (1984) J. A. Ramsey, K. R. Swartzel. J. Food Sci. *49*, 257-262.

Rates of sedimentation and fat separation were determined for stored UHT treated milk. For each of three thermal treatments used for indirect and direct heating, homogenization pressures were 0, 10.34, or 20.68 MPa. Storage temperatures were 7, 22 and 35° C. Initial sediment deposits were greater for the direct system. Sedimentation increased with increased heat treatment and/or storage temperature but

decreased as homogenization pressure increased. The indirect system had higher activation energies for sedimentation for all homogenization pressures. Fat separation rates tended to increase with increased storage temperature. The direct system tended to produce more sediment and less fat separation than the indirect system for a given thermal treatment.

High Vacuum Flame Sterilized Fruits: Influence of Can Type on Storage Stability of Vacuum Packed and Pear Slices. (1984) S. J. Leonard, J. R. Heil, P. A. Carroad, R. L. Merson, T. K. Wolcott. J. Food Sci. *49*, 263-266.

The feasibility of using enameled tin and tin-free steel (TFS) cans for processing oxygen sensitive fruits by high vacuum flame sterilization was evaluated. Through 18 months storage at ambient temperatures, the appearance and quality of the HVFS peaches and pears remained acceptable for all can types. Fruits packed into plain tin cans appeared brighter and tasted tangier than those packed into TFS or inside-enameled tin cans. Texture, pH and titratable acidity of fruit were not measurably affected by variation in can types. Mechanical deaeration followed by flame sterilization, produced a product with quality comparable to that achieved in flame deaerated packs.

Temperature Histories in a UHT Indirect Heat Exchanger. (1984) J. P. Adams, J. Simunovic, K. L. Smith. J. Food Sci. *49*, 273-277.

An indirect UHT processing system was modeled by a computer program to predict the temperature profile of a mass element of fluid as it progressed through heating, hold and cooling units. The computer program consisted of successive calculations of the temperature of the exit of numerous increments in each unit based on the overall heat transfer coefficient determined for the total length of the unit. The validity of the computer program was determined by correlation of computer results with experimental determinations of sucrose inversion. The percentage of total inversion of sucrose occuring in the heater was 36%, indicating the error associated with the assumption of chemical reactions based exclusively on hold tube temperature, residence time and laminar flow pattern.

Sorption Isotherms and Drying Rates of Jerusalem Artichoke (Helianthus Tuberosus) (1984) G. Mazza. J. Food Sci. *49*, 384-388.

Moisture sorption properties and drying behavior of Jerusalem artichoke roots were investigated. Sorption isotherms of dehydrated and freeze-dried material, its water insoluble components, fructose, glucose and sucrose were determined at 10, 25 and/or 40° C. Adsorption-desorption isotherms indicated a combination of sorption by soluble sugars, in the crystalline, amorphous and aqueous solution state, and sorption by polymeric material such as cellulose, inulin and protein. In drying experiments conducted at 50, 65, 80, and 95° C, and also at 65° C and four air velocities and four bed depths, it was found that temperature and drier load conditions are of critical importance to drying behavior, drying time and finished product color. Increasing the air

velocity from 2.0 to 4.2 m/sec, at a temperature of 65° C and a bed depth of 10.5 cm, did not change the rate for drying 1 cm cubes.

Apple Pomace Energy and Solids Recovery. (1984) W. J. Jewell, R. J. Cummings. J. Food Sci. *49*, 407-410.

Apple pomace is an excellent example of a wasted food resource which also causes significant disposal problems. Two unique apple pomace processing systems were found capable of converting this wasted residue into a beneficial resource. The first process anaerobically digested the pomace producing energy as biogas. Bench and pilot scale testing indicated that nearly 80% of the pomace organics could be converted into a substitute natural gas with an energy value of $10-$30 per wet metric ton. The second process, called "Bio-drying," combined a high rate composting reactor with a low energy consuming dryer. Operation of a full scale biodrying system achieved wet pomace mass and volume reductions greater than 70% and produced a dried, stable, odorless product in less than 5 days.

Degration of Wheat Starch in a Single Screw Extruder: Characteristic of Extruded Starch Polymers. (1984) F. J. Davidson, D. Paton, L. L. Diosady, G. Larocque. J. Food Sci. *49*, 453-458.

Wheat starch was processed in a 19 mm diameter, single screw extruder to study the physical and structural modifications that occur during extrusion cooking. Structural modification of the starch polymers was investigated using gel permeation chromatography (GPC), enzymatic digestions and dilute solution viscometry. Both the GPC and intrinsic viscosity results showed that the average molecular size significantly decreased as a result of extrusion processing. The relative amount of material excluded by Bio-Gel A150m was considerably lower for extruded samples than for unprocessed wheat starch and this size reduction of the amylopectin fraction was attributed to mechanical rupture of covalent bonds. The characterization of the structural modifications of the starch polymers is reported.

Sterilization of Food in Containers with an End Flat Against a Retort Bottom: Numerical Analysis and Experimental Measurements. (1984) D. Naveh, I. J. Pflug, I. J. Kopelman. J. Food Sci. *49*, 461-467.

The heating characteristics of a metal container (filled with a conduction heating food) heated with one end flat against a retort bottom was simulated numerically using the Finite Element method. Results of heat penetration tests in a laboratory retort and in a commercial crateless retort were compared to results obtained in computer simulations. It was observed that semilogarithmic heating curves are curved under the conditions described. It was also shown that the slowest heating zone moves towards the container bottom during heating. Heat flux, which is initially directed from the retort bottom towards the can, is reversed at long heating times; i.e., heat flows from the container to the retort bottom. Suggestions are given for the handling of this type of situation in commercial practice.

Parametric Analysis for Predicting Freezing Time of Infinitely Slab-Shaped Food. (1984) J. Succar, K. Hayakawa. J. Food Sci. *49*, 468-477.

A computer program was developed in order to predict freezing times of homogeneous food which may be approximated by infinite slabs. For this solution we assume temperature dependent thermophysical properties, together with symmetric or non-symmetric convective and radiative heat exchange imposed at the boundaries. Through appliation of a statistical analysis, all dimensionless groups that have a significant influence in the rate of heat transfer were selected and used to develop a regression equation for the prediction of freezing times, by applying a central composite experimental design. This equation is applicable to the wide range of parametric values encountered during commercial operations. The reliability of the computer program and regression equation developed was verified experimentally.

Thermodynamic and Kinetic Stability Constants of Selected Carboxylic Acids and Iron. (1984) J. E. Gorman, F. M. Clydesdale. J. Food Sci. *49*, 500-503.

Thermodynamic stability constants for complexes of lactic, malic, succinic and citric acids with both ferrous and ferric iron were determined. The rate of transfer of iron to apotransferrin, which has been defined as the kinetic stability constant, was also determined for both these and ascorbic acid complexes. The thermodynamic stability constants for malate and succinate were similar to ascorbate while that for lactate was somewhat lower. The kinetic stability constants in ascending order were as follows: lactate, ascorbate and malate, succinate and citrate. However, data from this study indicated that the slope of the initial portion of the iron exchange curves might be a better measure of potential bioavailability. In descending order the slopes were: ascorbate, lactate, malate, citrate, and succinate.

Effects of Water Activity Light Intensity and Physical Structure of Food on the Kinetics of Riboflavin Photodegradation. (1984) E. M. Furuya, J. J. Warthesen, T. P. Labuza. J. Food Sci. *49*, 525-528.

The kinetics of light-induced riboflavin degradation were evaluated in elbow macaroni, particulate macaroni, nonfat dried milk, skim milk and a buffered solution of riboflavin. A first order degradative mechanism was observed in liquid systems, while a two-phased mechanism was observed in dry food systems. Light intensities of 25, 50 or 100 ft-c showed no significant differences in effect on the rate of riboflavin loss in elbow macaroni; however, a very dim light showed only single-phased first order rate of loss. In elbow macaroni exposed to a broad range of water activities the degradation of riboflavin increased at elevated relative humidities. Lumichrome was determined to have limited use as a quantitative indicator of riboflavin loss, but could be used as a qualitative indicator of riboflavin degradation.

Effect of Water Activity on the Major Volatiles Produced in a Model System Approximating Cooked Meat. (1984) G. J. Hartman, J. D. Scheide, G. T. Ho. J. Food Sci. *49*, 607-613.

The effects of water activity (a_w) on the major volatiles produced from a meat flavor model system containing monosodium-L-glutamate, L-ascorbic acid, thiamin HCl and cystine was investigated. Quantitative and qualitative differences in volatiles produced between high and low a_w systems (heated at 135° C) were found. Qualitative changes were observed to occur at about a_w 0.4. Compounds identified in high and low a_w systems fell into classes which are associated with boiling and roasting cooking techniques (respectively) of known naturally occurring compounds.

Constitutive Relationship for Apple Cortex Under Hydrostatic Stress. (1984) A. K. Datta, C. T. Morrow. J. Food Sci. *49*, 623-627.

Hydrostatic creep tests were run on cylindrical specimens of Rome Beauty apples to study the mechanical response. Volumetric strain was measured for different levels and durations of applied stress. The former was separated into recoverable, permanent, instantaneous, and time dependent components. A general constitutive relationship was developed from statistical analysis. A mechanical model was proposed to explain the strain response of the material.

ABSTRACTS FROM TRANSACTIONS OF ASAE

The Effect of Bruising on Dried Fruit Quality. (1984) M. O'Brien, R. P. Singh, R. E. Garrett. Trans. ASAE *27*, 274-277.

Tests were made to determine the effect of bruising on dried fruit quality. When standard drying practices are followed the bruised portions of apples and pears suffer discoloration and collapse of cellular structure. The texture was "leathery" and the taste bland. Electron microscopic pictures of cell structure of bruised and unbruised fruit reveal rupture and cleavage of cell walls which result in release of enzymes that cause browning and lowering of quality.

Critical Strain Failure Criterion: Pros and Cons. (1984) Pictiaw Chen, Zongnan Sun. Trans. ASAE *27*, 278-281.

Critical strain has recently been proposed as a failure criterion for fruit tissue. This criterion is contradictory to the traditional belief that failure in fruit tissue is caused by either shear or normal stress, depending on the loading conditions. This paper presents arguments both for and against the critical-strain hypothesis. The arguments are based on results of our study and a review of the literature.

Microwave-Roasted Soybeans. (1984) E. D. Rodda, P. R. Hill, K. E. Harshbarger. Trans. ASAE *27*, 282-286.

Whole soybeans were presoaked to 20, 40 and 60% moisture contents in 0.5% sodium bicarbonate water solution. They were then cooked to a golden brown color in a microwave oven. The ground microwave-processed soybeans were fed as the only source of protein in 10% crude protein diets to young rats to study the effects of moisture content and methionine supplementation on protein nutritive value. The protein nutritive value was improved by increasing the precooking moisture content from 20 to 40 to 60%. Methionine supplementation improved growth responses at each moisture level. Trypsin inhibitor activity of the microwave-processed soybean products was very low compared to raw soybeans and differences in protein nutritive value were not due to presence of trypsin inhibitor.

A Mathematical Model of Produce Damage Mechanisms. (1984) K. Peleg. Trans. ASAE *27*, 287-293.

A mathematical model, enabling prediction of produce bruise size and depth of fruit deformation is developed. The maximal pressure at the center of the contact circle is also computed. The model assumes spherical fruit shape, and considers configurations of two fruits in contact, a fruit in contact with a rigid plane and a fruit in a spherial cup, such as in tray packs. The material properties of fruits are expressed in terms of the non-linear relaxation modulus while comparing results to the classical Hertz contact problem of perfectly elastic and linear viscoelastic spheres. Equations are developed for constant load forces, e.g., dead weight, continuous sinusoidally varying force, a transient force pulse and combinations thereof. These enable comparison of bruise size, caused by static and dynamic loads of the same magnitude.

Rheological Properties of Plain Egg Yolk, Salted Egg Yolk and Salted Whole Egg. J. G. Pitsilis, D. B. Brooker, O. J. Cotterill, H. V. Walton. Trans. ASAE *27*, 294-299.

The rheology of commercial plain and salted yolk and salted whole egg has been studied using rotational viscometers within a temperature range of 5 to 45° C. Shear rates of 37 to 300/s for the yolks and 37 to 250/s for the salted whole egg were used. Solid content ranged from 43% to 47% for plain egg yolk. Data were fitted to the power law model $\tau = KY^n$ and explicit expressions for the constants K and n were derived as functions of temperature and solid content.

Rheological Properties of Liquid Egg White. (1984) J. G. Pitsilis, D. B. Brooker, H. V. Walton, O. J. Cotterill. Trans. ASAE *27*, 300-304.

The flow behavior of commercial liquid egg white within a temperature range of 5 to 45° C and a shear rate range of 37 to 350/s has been studied using rotational viscometers. The power law model expressing shear stress as a function of shear rate was fit to the data and functions for K and n were derived. The constants K and n are explicit functions of temperature.

Failure Characteristics of Apple Tissue Under Cyclic Loading. (1984) N. B. McLaughlin, R. E. Pitt. Trans. ASAE *27*, 311-320.

This report is a study of the response of apple tissue to compressive cyclic loading. Experiments were performed in which cylindrical samples of apple tissue were subjected to cyclic loading, with the peak stress either remaining constant or slightly increasing with each cycle. For comparison, static loading tests were performed with comparable stress magnitudes. It was found that apple tissue can fail under cyclic or static loadings of magnitude insufficient to cause failure initially. Failure was apparently due to a propagation of cell wall ruptures in a plane perpendicular to the axis of the applied stress, as under ordinary constant-strain-rate tests. The failure characteristics in terms of tissue strength, strain at failure, and time to failure were not significantly different under cyclic and static loadings; however, the strain at failure was about 30% greater than that under constant-strain-rate loading. A statistical model for the number of cycles to failure indicates that the likelihood of imminent failure remained approximately constant with the number of cycles applied, and thus failure appeared to be primarily a random event rather than the result of damage accumulation. The results of a simple model of the parenchyma cell indicate that cell wall stresses are greatest in the initial appliation of load under cyclic or static loadings. Thus, it is theorized that the initiation of failure is caused by a random decay in cell wall strength under applied load.

Evaluation of Selected Mathematical Models for Describing Thin-Layer Drying of In-Shell Pecans. (1984) M. S. Chhinnan. Trans. ASAE *27*, 610-615.

An experimental dryer was designed and fabricated for thin layer drying studies of pecans. Thin layer drying data were obtained for in-shell pecans for 16 drying conditions involving four dry bulb temperatures (29.4, 35.0, 40.5 and 46.1° C) and four

dew point temperatures (8.9, 13.3, 17.8 and 22.2°C). Four mathematical models evaluated to fit the data were: One parameter exponential model, diffusion model, approximation of diffusion model and the Page equation. The Page equation was found to be most suitable in describing the drying characteristics of a single layer of in-shell pecans.

Pressure Drop Across Values and Fittings for Pseudoplastic Fluids in Laminar Flow. (1984) J. F. Steffee, I. O. Mohamed, E. W. Ford. Trans. ASAE *27*, 616-619.

Friction loss coefficients for applesauce flowing under laminar conditions were measured for an elbow, a tee (used as an elbow) and three-way plug valve. Results indicate that these coefficients increase significantly with decreasing values of the generalized Reynolds number. General design recommendations for estimating the pressure loss for pseudoplastic (shear-thinning) fluids flowing through values and fittings are presented.

Pea Blanching Data. (1984) E. C. Pereira, D. R. Thompson. Trans. ASAE *27*, 620-623.

Laboratory and production scale studies were conducted to determine the effects of blanching on early June and medium sweet peas. Variables monitored were gas removal, firmness, enzymatic activity, recovery and organoleptic quality.

Most changes occur in peas during the first 3 min of blanch at 96°C (205°F).

Green Bean and Asparagus Blanching Data. 1984. E. C. Pereira, J. Norwig, D. R. Thompson. Trans. ASAE *27*, 624-628.

The effects of blanching on asparagus and cut green beans were determined by measuring gas removal and recovery after blanch. Canned beans were also examined for changes after storage. Gas removal from the asparagus was almost complete after the first minute of blanch and increased with blanch temperature. All changes in green beans are nearly complete in a 3-min blanch at 82°C (180°F).

Problems in Using Apparent Viscosity to Select Pumps for Pseudoplastic Fluids. (1984) J. F. Steffe. Trans. ASAE *27*, 629-634.

Using an apparent viscosity value and assuming Newtonian flow behavior is a commonly practiced method of estimating pressure losses for the flow of pseudoplastic (shear-thinning) fluids in tubes. This procedure may lead to significant over or under estimation in pressure loss and power requirements depending on the rate of shear at which the apparent viscosity is determined. These problems may result in large errors in analyzing the performance of fluid handling systems and lead to improper sizing of pumps and motors.

Adsorption Characteristics of Bentonite and Its Use in Drying Inshell Pecans. (1984) S. R. Ghate, M. S. Chhinnan. Trans. ASAE *27*, 635-640.

Adsorption characteristics of three types of calcium bentonite were evaluated at 15° C, 27° C and 36° C for 10% to 75% relative humidity environments obtained with saturated salt solutions. In general, all bentonites had the equilibrium moisture content (dry basis) of about 6% at 12% r.h. and 17% at 75% r.h. Freshly harvested inshell pecans were kept in direct contact with bentonites by mixing bentonites into pecans in various proportions. Desired drying was achieved within 48 h. The quality of bentonite dried inshell pecans was equal to those dried in the laboratory in static ambient environment.

Improving the Air Flow Distribution in a Batch Walnut Dryer. (1984) T. R. Rumsey, T. Fortis. Trans. ASAE *27*, 938-941.

English walnuts are usually dried on farm in batch dryers. Field measurements have shown that non-uniform air flow patterns exist in one common type of bulk dryer. These non-uniform air flows are the suspected cause of non-uniform drying that has been observed by some walnut growers. A two-dimensional finite element model has been used to evaluate modifications to improve the air flow distribution within the drying bins.

Ambient Air Drying of English Walnuts. (1984) T. Rumsey, J. Thompson. Trans. ASAE *27*, 942-945.

Most English walnuts in California are dried on farm in batch dehydration systems. The drying season lasts from September through the end of October. Heated air, at temperatures up to 43° C, is forced through the fixed bed dryers. Temperatures above 43° C will cause oil in the nut meat to become rancid (Woodroof, 1978). The initial moisture content of the nuts ranges from 15 to 50% (dry basis), and they are required to be dried to 8.7%.

Due to increasing energy costs and scarcity of fuel supplies, research into natural air drying of walnuts was started at the Agricultural Engineering Department at the University of California in 1977 (Thompson et al., 1978). Initial field trials showed the feasibility of drying walnuts with ambient air. The drying times were longer, but there were no signs of deterioration of nut quality.

A second phase of the project has been to modify a grain drying simulation computer program to model walnut drying. The program modified was the Michigan State University fixed bed grain drying program (Bakker-Arkema *et al.* 1974). This paper describes the modifications that were made, and compares results predicted by the model to field drying tests. The model was used to simulate ambient air drying at three walnut growing locations in California.

Product Yield From on the Rail Boning of Hot and Chilled Sides from Forage-Fed Cattle. (1984) C. F. Brasington, D. M. Stiffler, Cl. L. Griffin, G. C. Smith. Trans. ASAE. *27*, 946-949.

Carcass sides were obtained from the slaughter of 33 forage-fed mixed-breed steers. The carcasses received an average USDA yield grade of 29, a quality grade of high standard, and a skeletal and lean maturity score of "A". The average hot carcass weight was 265 kg. The mean yield percentage of boneless meat when removed hot was 0.99 greater ($P < 0.01$) than that of carcasses chilled boned after 24 h in a cooler at 2° C. A comparison of the mean weights for hot- and chilled-boned products shows that the hot-boned yield was higher for 12 of the 16 meat cuts and lean trim listed. The mean yield weight of boneless meat per equivalent carcass was 199.74 kg for hot-boned sides and 197.32 kg for chilled-boned sides. The mean shrink for hot-boned sides was 1.42% less than that for chilled-boned sides.

Energy from Cull Fruit. (1984) D. J. Hills, D. W. Roberts. Trans. ASAE. *27*, 1240-1244.

A 12-month investigation was conducted to study energy extraction from fruit residue. Cull fruits were fermented to produce ethanol, the ethanol was distilled off from the resulting beer, and the stillage was anaerobically digested to produce methane. During the first eight months, laboratory scale studies were conducted on cull fruit samples (apple, cantaloupe, grape, honeydew, orange, peach, pear, and plum). Samples were fermented in 4-L batch fermentors; the ethanol was subsequently removed from the solutions using a laboratory still; finally, the stillages were digested using 4-L batch anaerobic digesters. During the latter four months of the investigation peach culls were processed in a pilot size, batch mode, ethanol plant. The resulting stillages were fed to a 100-L, continuous mode, anaerobic digester. Sufficient methane gas was produced from the majority of the stillage tested to meet distillation energy requirements.

Design of a Microcomputer-Based Instrument for Crispness Evaluation of Food Products. (1984) S. K. Seymour, D. D. Hamann. Trans. ASAE. *27*, 1245-1250.

An instrument costing under $4000 was built to study the acoustical properties of crisp foods. A spectrum analyzer was built around an Apple II+ microcomputer (Apple Computer, Inc.) for analyzing acoustical frequencies in the 0.5 to 3.3 kHz range. The instrument was evaluated with sine and square waves of known amplitudes and frequencies. Samples of Pringles potato chips were crushed and their sound output recorded. Sound pressure level spectra were later developed by the instrumentation.

FNP

JOURNALS AND BOOKS IN FOOD SCIENCE AND NUTRITION

Journals

JOURNAL OF FOODSERVICE SYSTEMS, O. P. Snyder, Jr.

JOURNAL OF FOOD BIOCHEMISTRY, H. O. Hultin, N. F. Haard and J. R. Whitaker

JOURNAL OF FOOD PROCESS ENGINEERING, D. R. Heldman

JOURNAL OF FOOD PROCESSING AND PRESERVATION, D.B. Lund

JOURNAL OF FOOD QUALITY, M. P. De Figueiredo

JOURNAL OF FOOD SAFETY, M. Solberg and J. D. Rosen

JOURNAL OF TEXTURE STUDIES, M. C. Bourne and P. Sherman

JOURNAL OF NUTRITION, GROWTH AND CANCER, G. P. Tryfiates

Books

NEW DIRECTIONS FOR PRODUCT TESTING AND SENSORY ANALYSIS OF FOODS, H. R. Moskowitz

PRODUCT TESTING AND SENSORY EVALUATION OF FOODS, H. R. Moskowitz

ENVIRONMENTAL ASPECTS OF CANCER: ROLE OF MACRO AND MICRO COMPONENTS OF FOODS, E. L. Wynder *et al.*

FOOD PRODUCT DEVELOPMENT IN IMPLEMENTING DIETARY GUIDELINES, G. E. Livingston, R. J. Moshy, and C. M. Chang

SHELF-LIFE DATING OF FOODS, T. P. Labuza

RECENT ADVANCES IN OBESITY RESEARCH, VOL. III, P. Bjorntorp, M. Cairella, and A. N. Howard

RECENT ADVANCES IN OBESITY RESEARCH, VOL. II, G. A. Bray

RECENT ADVANCES IN OBESITY RESEARCH, VOL. I, A. N. Howard

ANTINUTRIENTS AND NATURAL TOXICANTS IN FOOD, R. L. Ory

UTILIZATION OF PROTEIN RESOURCES, D. W. Stanley, E. D. Murray and D. H. Lees

FOOD INDUSTRY ENERGY ALTERNATIVES, R. P. Ouellette, N. W. Lord and P. E. Cheremisinoff

VITAMIN B_6: METABOLISM AND ROLE IN GROWTH, G. P. Tryfiates

HUMAN NUTRITION, 3RD ED., F. R. Mottram

DIETARY FIBER: CURRENT DEVELOPMENTS OF IMPORTANCE TO HEALTH, K. W. Heaton

FOOD POISONING AND FOOD HYGIENE, 4TH ED., B. C. Hobbs and R. J. Gilbert

POSTHARVEST BIOLOGY AND BIOTECHNOLOGY, H. O. Hultin and M. Milner

THE SCIENCE OF MEAT AND MEAT PRODUCTS, 2ND ED., J. F. Price and B. S. Schweigert

GUIDE FOR AUTHORS

Typewritten manuscripts in triplicate should be submitted to the editorial office. The typing should be double-spaced throughout with one-inch margins on all sides.

Page one should contain: the title, which should be concise and informative; the complete name(s) of the author(s); affiliation of the author(s); a running title of 40 characters or less; and the name and mail address to whom correspondence should be sent.

Page two should contain an abstract of not more than 150 words. This abstract should be intelligible by itself.

The main text should begin on page three and will ordinarily have the following arrangement:

Introduction: This should be brief and state the reason for the work in relation to the field. It should indicate what new contribution is made by the work described.

Materials and Methods: Enough information should be provided to allow other investigators to repeat the work. Avoid repeating the details of procedures which have already been published elsewhere.

Results: The results should be presented as concisely as possible. Do not use tables *and* figures for presentation of the same data.

Discussion: The discussion section should be used for the interpretation of results. The results should not be repeated.

In some cases it might be desirable to combine results and discussion sections.

References: References should be given in the text by the surname of the authors and the year. *Et al.* should be used in the text when there are more than two authors. All authors should be given in the Reference section. In the Reference section the references should be listed alphabetically. See below for style to be used.

DEWALD, B., DULANEY, J. T. and TOUSTER, O. 1974. Solubilization and polyacrylamide gel electrophoresis of membrane enzymes with detergents. In *Methods in Enzymology,* Vol. xxxii, (S. Fleischer and L. Packer, eds.) pp. 82–91, Academic Press, New York.

HASSON, E. P. and LATIES, G. G. 1976. Separation and characterization of potato lipid acylhydrolases. Plant Physiol. *57,* 142–147.

ZABORSKY, O. 1973. *Immobilized Enzymes,* pp. 28–46, CRC Press, Cleveland, Ohio.

Journal abbreviations should follow those used in *Chemical Abstracts.* Responsibility for the accuracy of citations rests entirely with the author(s). References to papers in press should indicate the name of the journal and should only be used for papers that have been accepted for publication. Submitted papers should be referred to by such terms as "unpublished observations" or "private communication." However, these last should be used only when absolutely necessary.

Tables should be numbered consecutively with Arabic numerals. The title of the table should appear as below:

Table 1. Activity of potato acyl-hydrolases on neutral lipids, galactolipids, and phospholipids

Description of experimental work or explanation of symbols should go below the table proper. Type tables neatly and correctly as tables are considered art and are not typeset. Single-space tables.

Figures should be listed in order in the text using Arabic numbers. Figure legends should be typed on a separate page. Figures and tables should be intelligible without reference to the text. Authors should indicate where the tables and figures should be placed in the text. Photographs must be supplied as glossy black and white prints. Line diagrams should be drawn with black waterproof ink on white paper or board. The lettering should be of such a size that it is easily legible after reduction. Each diagram and photograph should be clearly labeled on the reverse side with the name(s) of author(s), and title of paper. When not obvious, each photograph and diagram should be labeled on the back to show the top of the photograph or diagram.

Acknowledgments: Acknowledgments should be listed on a separate page.

Short notes will be published where the information is deemed sufficiently important to warrant rapid publication. The format for short papers may be similar to that for regular papers but more concisely written. Short notes may be of a less general nature and written principally for specialists in the particular area with which the manuscript is dealing. Manuscripts which do not meet the requirement of importance and necessity for rapid publication will, after notification of the author(s), be treated as regular papers. Regular papers may be very short.

Standard nomenclature as used in the engineering literature should be followed. Avoid laboratory jargon. If abbreviations or trade names are used, define the material or compound the first time that it is mentioned.

EDITORIAL OFFICE: Dr. D. R. Heldman, Editor, Journal of Food Process Engineering, Campbell Institute for Research and Technology, Campbell Place, Camden, New Jersey 08101 USA.

CONTENTS